Univerzita Karlova v Praze

Matematicko-fyzikální fakulta

**DIPLOMOVÁ PRÁCE**


Bc. Zuzana Vidláková

# Studium kanálu J/Psi + foton v proton-protonových srážkách pomocí detektoru ATLAS na LHC

Ústav částicové a jaderné fyziky

Vedoucí diplomové práce: prom. fyz. Václav Vrba, CSc.

Studijní obor: Jaderná a subjaderná fyzika

Praha 2012

Prohlašuji, že jsem tuto diplomovou práci vypracovala samostatně a výhradně s použitím citovaných pramenů, literatury a dalších odborných zdrojů.

Beru na vědomí, že se na moji práci vztahují práva a povinnosti vyplývající ze zákona č. 121/2000 Sb., autorského zákona v platném znění, zejména skutečnost, že Univerzita Karlova v Praze má právo na uzavření licenční smlouvy o užití této práce jako školního díla podle § 60 odst. 1 autorského zákona.

V Praze dne 2.8.2012 Podpis autora

Název práce: Studium kanálu J/Psi + foton v proton-protonových srážkách pomocí detektoru ATLAS na LHC

Autor: Bc. Zuzana Vidláková

Katedra/Ústav: Ústav částicové a jaderné fyziky

Vedoucí diplomové práce: prom. fyz. Václav Vrba, CSc., Akademie věd České republiky

Abstrakt: V diplomové práci se zabývám fyzikou týkající se kvarkonií a jejich studiem pomocí detektoru ATLAS umístěného na urychlovači LHC v Ženevě. Práce pokrývá následující témata: základní údaje o detektoru ATLAS, historii spojenou s kvarkonii, jejich spektroskopií a produkčními mechanismy kvarkonií, sofware používaný v CERN k analýze dat, studium účinného průřezu J/Psi + foton kontinua. Analýza byla zpracována pro B-fyzikální pracovní skupinu kolaborace ATLAS.

Klíčová slova: CERN, LHC, ATLAS, B-fyzika, kvarkonia

Title: Analysis of J/Psi + photon production in proton-proton collisions on ATLAS at LHC

Author: Bc. Zuzana Vidláková

Department: Institute of particle and nuclear physics

Supervisor: prom. fyz. Václav Vrba, CSc. (Academy of Sciences of the Czech Republic)

Abstract: The subject of this thesis is physics connected to quarkonia and their studies at the ATLAS detector situated at LHC in CERN, Geneva. In this thesis, following topics are covered: ATLAS detector, history of physics connected to quarkonia, production mechanisms of quarkonia, software used at CERN for data analysis and cross-section measurement of J/Psi + photon continuum. The analysis was done on behalf of the B-physics working group at ATLAS.

Keywords: CERN, LHC, ATLAS, B-fyzika, quarkonia

# Contents

# 1 The Large Hadron Collider

The *Large Hadron Collider* (LHC) provides high-energy protons for collisions and the subsequent fragments are measured in detectors which are situated along the LHC ring. LHC is at the moment the largest and most powerful accelerator in the world.

The concept of this proton-proton collider was proposed in 1980s. More than 20 years later in September 2008 the LHC was ready to start its hunt for new physics phenomena. Shortly after putting into service a serious problem with one of the superconducting magnets occurred. This accident led to a disruption of a fine-tuned vacuum system and caused damage to a significant part of the machine. After the repairs, the second LHC commissioning took place in November 2009.

LHC is only the last and the biggest part of the chain of accelerators which are depicted in the figure 1. The hydrogen atoms are used as a source of protons. Protons are accelerated in the *Linac2* (linear accelerator) to the energy of 50 MeV. Then they are injected into *The Proton Synchrotron Booster* which accelerates them up to 1.4 GeV.

The nominal center-of-mass energy at the LHC is $\sqrt{s} = 14$ TeV. The beam of particles is not continuous, it is separated into 2808 bunches in each beam. Every bunch contains approximately $1.15 \times 10^{11}$ protons and the LHC is designed for 25 ns bunch separation in the ring.

Such collider can be used not only to maintain, accelerate and collide protons, but also heavy ions. This possibility was part of the conceptual design from the early stages of the whole project. One month of every LHC operational year is dedicated to collisions of fully stripped lead ions ($^{208}\mathrm{Pb}^{82+}$). The aim of nucleon-nucleon collisions studies is to reveal the physical behaviour of strongly interacting matter at extreme energy densities where the formation of a new phase of matter, the quark–gluon plasma, is expected. The measurements of quark-gluon plasma are very important for understanding of some topics connected to Quantum Chromodynamics like confinement or chiral-symmetry restoration. The ALICE (A Large Ion Collider Experiment) detector is primarily dedicated to this task.

The use of proton-proton beams was favoured for two main reasons: The first is that in a curved magnetic field charged particles are losing energy due to the synchrotron radiation according to the equation

$$E_{loss} = \frac{1}{6\pi\epsilon_0}\frac{E^4}{\rho^2}\frac{e^2 c}{m^4 c^8}, \tag{1}$$

where $E$ is the proton energy, $e$ stands for the electron charge, $c$ for the speed of light, $\epsilon_0$ for vacuum permittivity, $m$ for the particle mass and $\rho$ for the the bending radius. Now it is obvious that the energy losses depends on the mass of the accelerated particle, the smaller

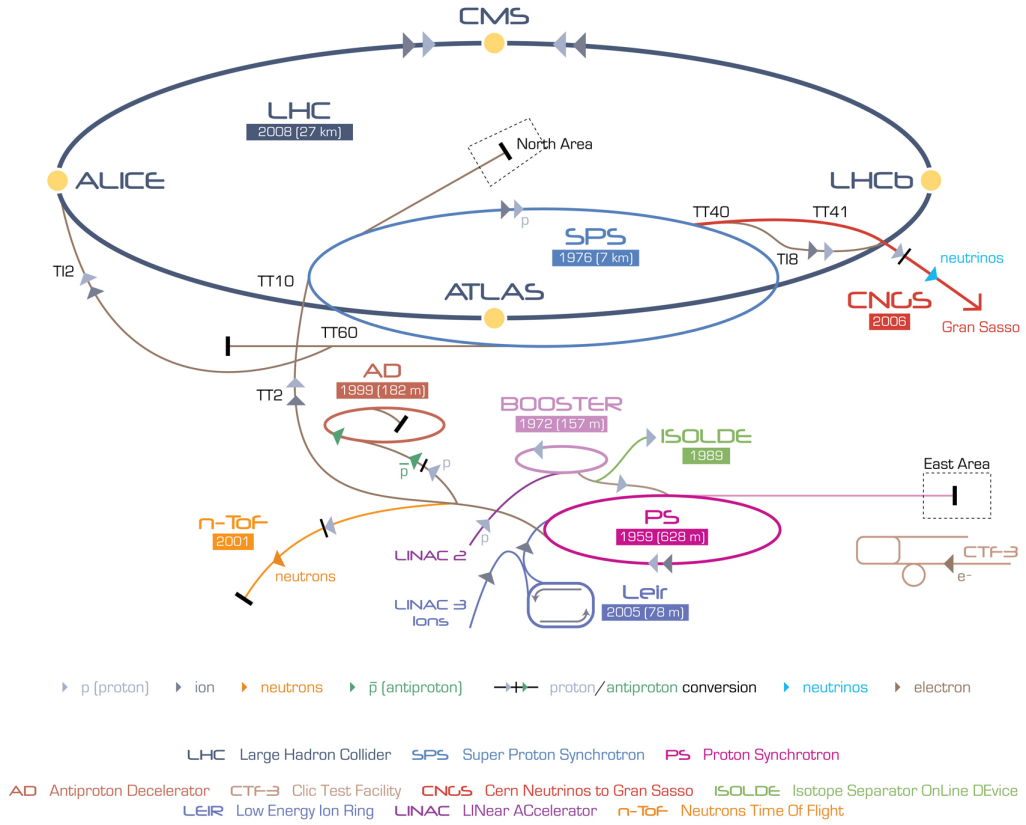


Figure 1: The complex of accelerators and the LHC with four main experiments [AccComp].

the mass, the higher is the radiation. It implies that electrons can be accelerated to a limited energy at circular colliders.

It would be also easier to make proton-anti-proton collider. In this case only one system of magnets and beam pipes is needed. However it is not trivial to make high-intense anti-proton beams. Finally, a decision was made to develop a composite design of superconducting magnets to deploy two separate beam pipes.

Here should be noted that the proton bunches also produce synchrotron radiation at increasing amplitude and frequency as they are accelerated in vacuum. Protons produce photoelectrons which in turn propagate secondary electrons from the pipe walls with increasing frequency and density up to $7 \times 10^{10}$. Each proton loses this way ~6.7 keV per turn.

There are several quantities frequently used in high-energy physics and are important for proper understanding of this thesis. The first is called total *integrated luminosity* $\mathcal{L}$ which express number of collisions which produce the particular process $N$ that are delivered into detector divided by cross section $\sigma$ of the process

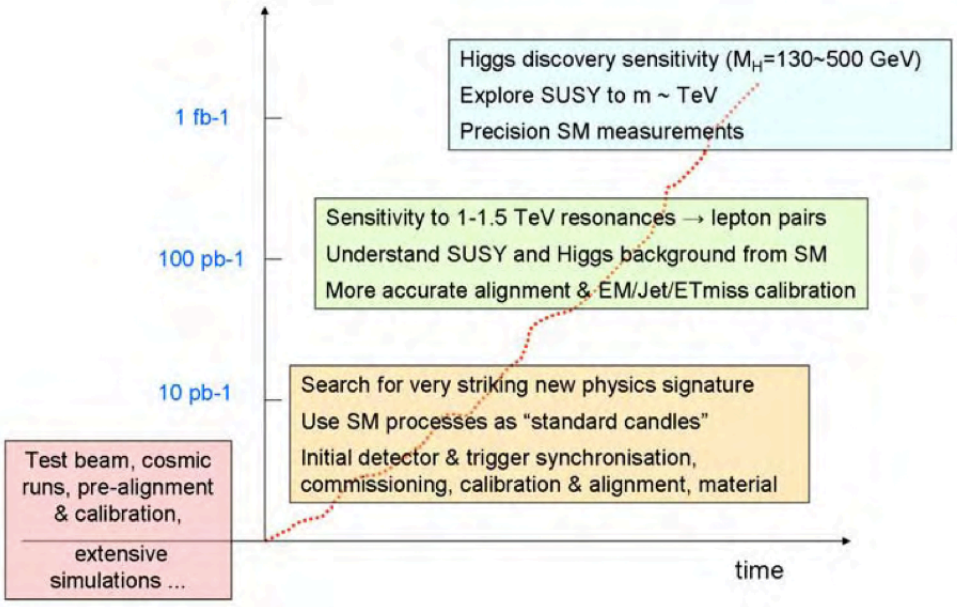


Figure 2: Plan of the physics analysis at LHC [PhysOut].

$$\mathcal{L} = \frac{\sigma}{N}. \tag{2}$$

In the figure 2, can be found a general plan for the physics analysis at LHC as it will proceed with increasing luminosity.

The total recorded luminosity in 2011 run of ATLAS detector was 5.25 $\text{fb}^{-1}$ [Lum]. The following values are closely connected to the coordinate system of ATLAS. The ATLAS collaboration is using standard right-handed coordinate system. The $x$-axis is pointing towards the center of the LHC ring. The $y$-axis is pointing up to the surface and it slightly differs from vertical axis. Then the $z$-axis copies the beam direction.

The *pseudorapidity* $\eta$ of particle from primary vertex is defined as

$$\eta = -\ln \tan \frac{\theta}{2}, \tag{3}$$

where $\theta$ is angle measured from positive $z$-axis in $zx$ plane.

Pseudorapidity is close to the *rapidity* $y$ but rapidity additionally depends on the energy $E$ of the particle and for the needs of the particle physics it is relative to the beam axis $z$

$$y = \frac{1}{2} \ln \frac{E + p_L c}{E - p_L c}, \tag{4}$$

where $p_L$ denotes longitudinal component of momentum along the $z$-axis. The rapidity defined this way express rapidity of the boost along the beam axis which takes an observer from the lab frame to a frame in which the particle moves only perpendicularly to the beam.

To measure the angular distance between two objects, one object with coordinates $(\eta_1, \phi_1)$ and the other with $(\eta_2, \phi_2)$, is used so called *angular distance* $\Delta R$

$$\Delta R = \sqrt{(\phi_1 - \phi_2)^2 + (\eta_1 - \eta_2)^2}. \tag{5}$$

The *transverse momentum* $p_T$ is the component of momentum in the transverse plane $xy$

$$p_T = p \sin \theta. \tag{6}$$

In the following text the mass will be denoted for short keV, MeV GeV, etc. instead of KeV/c$^2$, MeV/$^2$, GeV/$^2$, etc.

# 2 ATLAS experiment

ATLAS (A Toroidal LHC ApparatuS) is one of four main detectors at the LHC. The assembling of the ATLAS detector started in 2003 and it took 4 years to have all the parts put together. It is a general-purpose detector which was designed to take advantage of the full discovery potential of the LHC. Data obtained online by the ATLAS are further analysed in order to search for the Higgs boson, SUSY particles, B–physics studies, etc.

ATLAS consist of four main sub-detectors: the *Inner detector* measures tracks of charged particles, the *Electromagnetic* and *Hadronic Calorimeters* obtain information about particles energy and the *Muon Spectrometer* measures properties of muons – particles that can penetrate matter easily and are not absorbed in the calorimeters. I described in details the components and parameters of the ATLAS in my bachelor thesis, *Trigger in the ATLAS experiment*. In the following chapters, I intend to present short overview of the most important parts of the ATLAS detector to provide a basic information, relevant to the physics analysis presented, for an reader that is unfamiliar with this detector. Even more thorough description can be found in [TDR] and [TDR2].

## 2.1 Inner Detector

The high-precision tracking and vertexing in environment with numerous tracks and primary vertices is ensured by the Inner Detector. It is the innermost detection system and it consists of three subdetectors: Pixel Detector, Semiconductor Tracker (SCT) and Transition Radiation Tracker (TRT).

The Pixel detector contributes at most to accurate measurements of vertices. The SCT determines precisely the particles momenta. The TRT is dedicated to pattern recognition with its good resolution of large number of close hits and it also contributes to the recognition of electrons.

### Pixel Detector

The Pixel Detector is the innermost part of the Inner detector. In general the Pixel detector consist of three cylindrical layers that form *barrel* part and three disks in the forward and backward region called *endcaps*. The first and very special layer which is situated only $\approx 5$ cm from the beam is called the B-layer. Altogether it contains 1744 pixel modules which function is to register charged particles. One pixel module is approximately 7 cm long and 2 cm wide. Hence the system provides three precision measurements in depth over the full acceptance. By combination of the hit signals from all layers the reconstructed particle

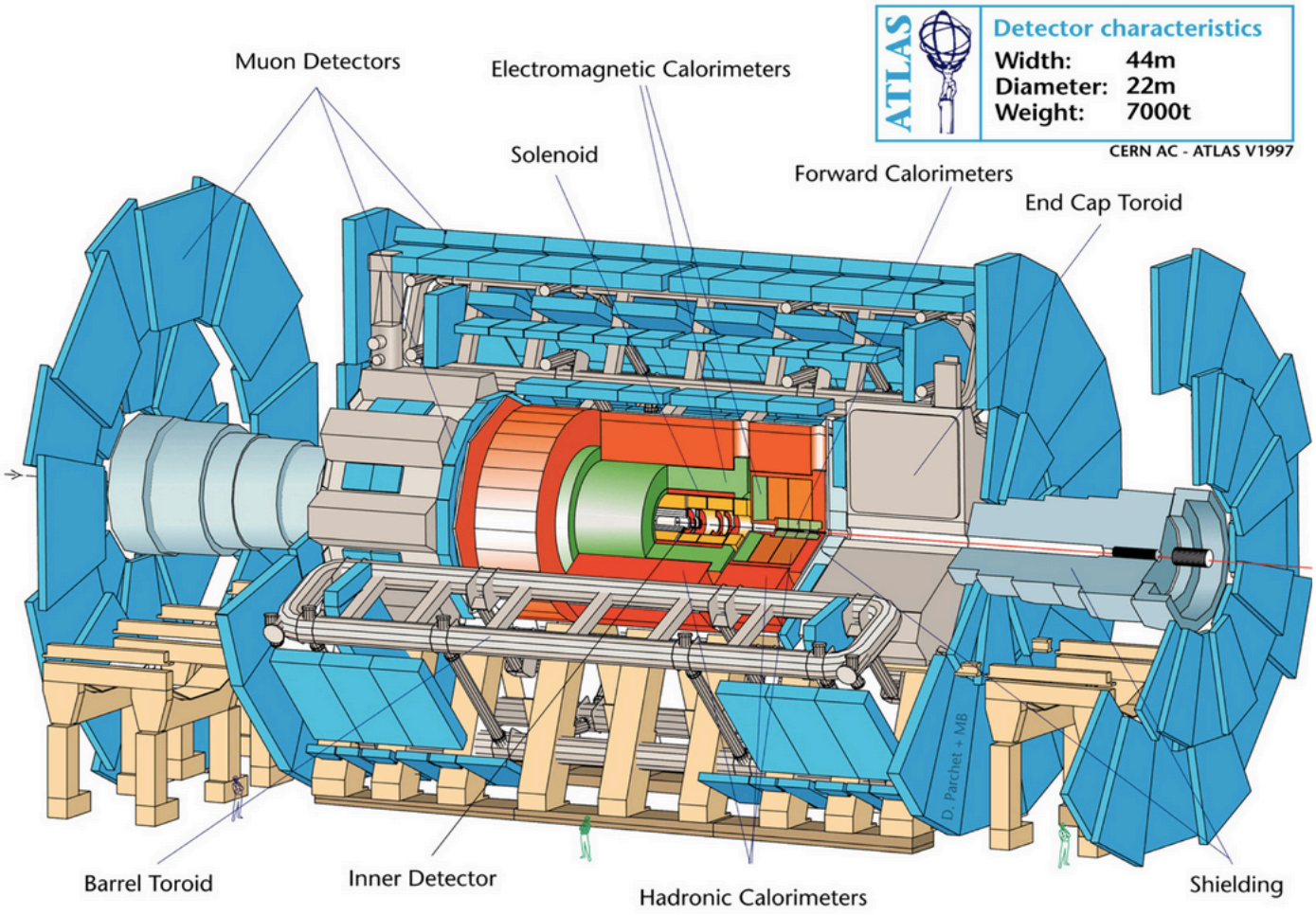


Figure 3: The ATLAS detector [ATLAS].

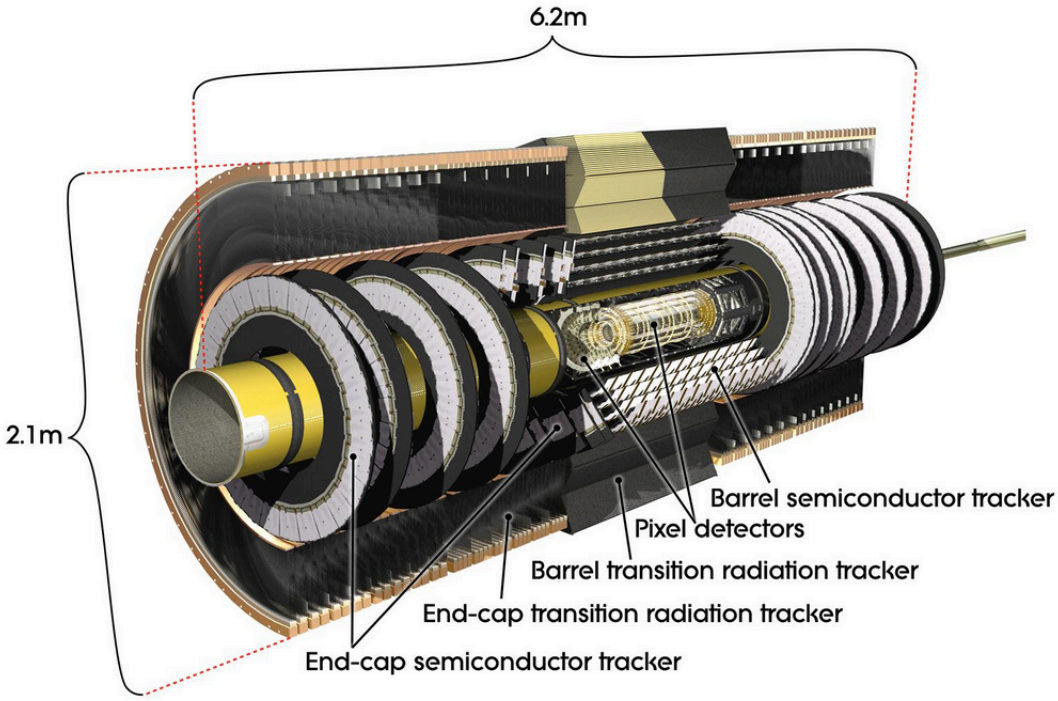


Figure 4: Structure of the Inner detector [Inner].

tracks can be gathered. The precise tracking allowes to achieve very good impact parameter resolution and it helps of to find short lived particles such as B-Hadrons. All important parameters of the Pixel Detector are listed in table 1.

### Semiconductor Tracker

The SCT has very similar purpose as the Pixel Detector, it differs only in the technology of silicon strips that are used to record particle tracks. Every SCT layer has two active sides and the whole subdetector has 8 strip layers.The strength of SCT lies in very precise measurement of hits in the $\phi$ direction but for a price of worse precision in measurements of $z$-coordinate that is parallel with LHC beam. The measurement of $z$-coordinate is possible because of the shift in position between two strips that lies upon each other. This means that every passing particle leaves four hits in the SCT. For important parameters of Semiconductor Tracker see table 1.

| System | Size of basic unit | Resolution | $\eta$ coverage |
|---|---|---|---|
| Pixel | $50 \times 40$ $\mu$m | $\sigma_{R\phi}$ = 14 $\mu$m<br>$\sigma_z$= 87 $\mu$m<br>$\sigma_R$= 87 $\mu$m | $\pm$2.5 |
| SCT | 12 cm $\times$ 112.5 $\mu$m<br>12 cm $\times$ 75 $\mu$m | $\sigma_{R\phi}$ = 15 $\mu$m<br>$\sigma_z$ = 770 $\mu$m | $\pm$2.5 |
| TRT | d = 4 mm<br>150 cm length | $\sigma_{R\phi}$ = 170 $\mu$m | $\pm$ 2.0 |

Table 1: The summary of size, resolution and $\eta$ coveradge of the Inner Detector subdetector.

### Transition radiation tracker

The TRT is the outermost part of the Inner Detector. It consist of straw detectors that basically are xenon-filled tubes with central gold-plated W-Re wire. The diameter of one straw is about 4 mm and the central wire placed in the center of each of them, has diameter of 30 $\mu$m and the length between 75 to 144 cm. The length varies if it is situated in the end-cap or the barrel region. The purpose of TRT is to detect photons radiated in passage of high-energetic particles as they traverse through the detector material. This helps to identify electrons from pions (or other hadrons) as they produce different numbers of transition radiation photons. TRT is able to detect in average $\approx$36 hits for every particle which also helps to to increase robustness and precision of the momentum measurements. For important parameters of Transition Radiation Tracker see table 1.

## 2.2 Calorimetry

The main purpose of the calorimetry at ATLAS is to provide information on energy of passing hadrons, photons, electrons and positrons. This cannot be assured by one calorimetric system, it requires at least two: one for the hadrons – the *Hadronic calorimeter* and the other for the rest of the particles – *Electromagnetic calorimeter*. To obtain the information about whole particle energy, the particle has to be stopped in the volume of the calorimeter. Therefore calorimeters have usually very high density to force particles to produce electromagnetic or hadronic showers that occur as they pass through and interact with particles of the absorber material. The ATLAS calorimeters have large pseudorapidity coverage of $|\eta| < 4.9$ to capture as much decay products as possible.

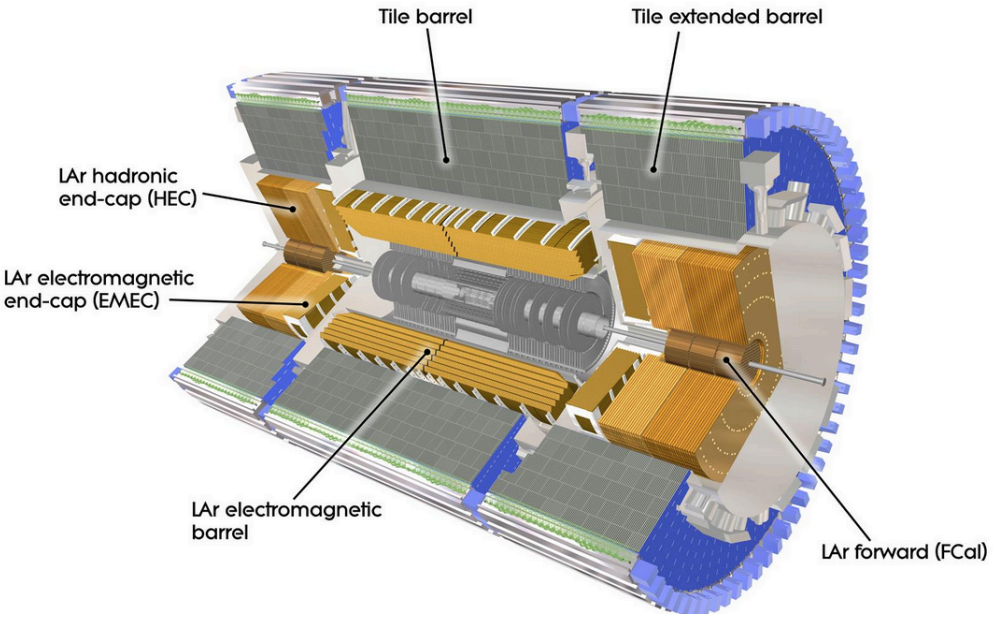


Figure 5: Scheme of calorimetry system at ATLAS [Calorimetry].

### Electromagnetic calorimeter

*The Electromagnetic liquid-argon calorimeter* (LAr calorimeter) in combination with lead absorber has very high granularity which allows the measurement of electron and photon transverse energy with high precision.

The kapton electrodes have shape of accordion which in combination with lead absorber provide it with complete $\phi$ symmetry without azimuthal cracks. The most precise measurements are specially demanded in the region of $|\eta| < 2.5$, where the EM calorimeter is longitudinally segmented in three sections in depth. The rest of the calorimeter is segmented in two sections in depth and has coarser lateral granularity. The total thickness of the EM calorimeter is over 22 radiation lengths $X_0$ in the barrel and $> 24\, X_0$ in the end-caps.

### Hadronic calorimeters

Hadronic calorimeter consist of three parts that are illustrated in the figure 5: the Tile calorimeter, LAr hadronic end-cap (HEC) calorimeter and LAr forward calorimeter. *The Tile calorimeter* (TileCal) is placed just outside the EM calorimeter. Its barrel covers the region $|\eta| < 1.0$, and its two extended barrels cover range $0.8 < |\eta| < 1.7$. The Tile calorimeter is a sampling calorimeter. In such calorimeter, steel is used as absorber material and scintillating plates read out by wavelength shifting (WLS) fibers as the active medium. It consists of

towers which have size $0.1 \times 0.1$ in $\Delta\eta$ and $\Delta\phi$.

The Tile calorimeter has high granularity and it provides also very quick response which makes it a best suited instrument for trigger. The barrel part is divided azimuthally into 64 modules and it is segmented in depth in three layers.

The *LAr hadronic end-cap* (HEC) is situated in the end-caps and instead of lead it uses copper as stopping material and liquid argon as active medium. In every end-cap are two independent wheels of HEC. It is located directly behind the end-cap electromagnetic calorimeter and they share the same LAr cryostats. To reduce the drop in material density at the transition between the end-cap and the forward calorimeter (around $|\eta| = 3.1$), the HEC is extended to $|\eta| = 3.2$ to overlap with the forward calorimeter. The situation is similar at the HEC where the $\eta$-range also slightly overlaps with the Tile calorimeter.

The *Forward calorimeter* (FCal) is made of copper and tungsten. FCal is designed to detect all particles with large pseudorapidity therefore it is located very close to the beam-pipe. It sits in the end-cap cryostats which provide benefits in terms of uniformity of the calorimetric coverage and reduced radiation background levels in the muon spectrometer. This calorimeter is approximately 10 interaction lengths long, and consists of three parts in each end-cap: the first copper module is optimised for electromagnetic measurements, while the other two tungsten. FCal is designed to measure the energy of hadronic interactions.

### Muon Spectrometer

Muons are able to cross the ATLAS inner volume almost undetected because they are the minimum ionizing particles (MIP). But hey are also important final products of many interesting particle decays. Therefore at ATLAS, the biggest and outermost part is formed by the muon spectrometers which measure muons momenta with high precision. Moreover the is also very important for triggering.

The muon spectrometry is based on the magnetic deflection of muon tracks in the large superconducting air-core toroid magnets. The barrel toroid provides the bending of incoming muons over the range $|\eta| < 1.4$. For $1.6 < |\eta| < 2.7$, the muon tracks are bent by two smaller end-cap magnets inserted into both ends of the barrel toroid. In the transition region ($1.4 < |\eta| < 1.6$), magnetic deflection is provided by a combination of barrel and end-cap fields. This set-up provides a field which is mostly orthogonal to the muon trajectories and minimises the resolution worsening due to multiple scattering.

In the barrel region, tracks are measured in chambers that are arranged in three cylindrical layers around the beam axis. In the transition and end-cap regions, the chambers are installed also in three layers in planes perpendicular to the beam. Over most of the $\eta$-range, a precision measurement of the track coordinates in the principal bending direction of the

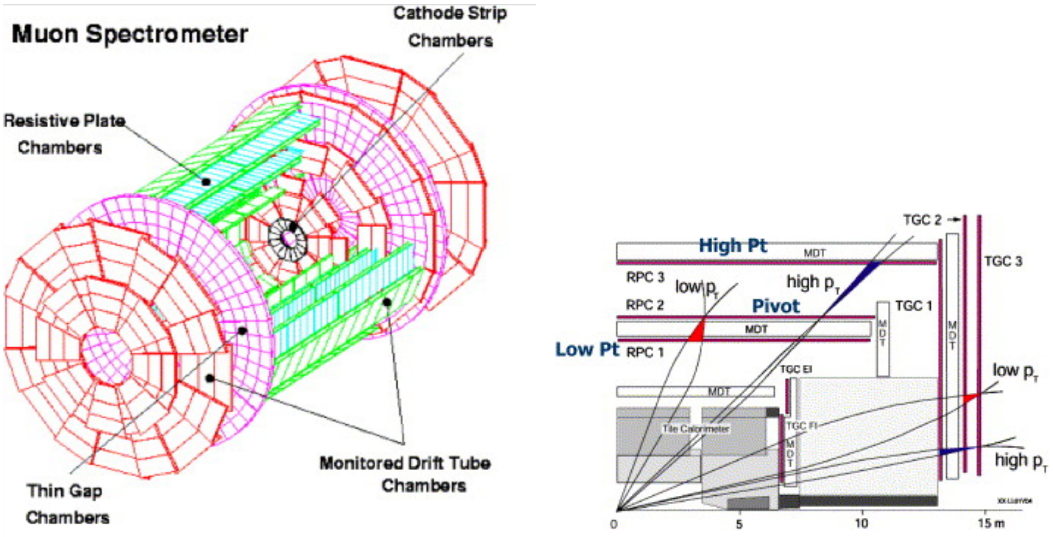


Figure 6: Scheme of the Muon Spectrometer (left). The geometry of muon tracks giving a muon trigger. (right). Both figures were taken from [MuTrig].

magnetic field is provided by *Monitored Drift Tubes* (MDTs). The multi-wire proportional chambers with cathodes that are segmented into strips are called *Cathode Strip Chambers* (CSC) and used at large pseudorapidities. To withstand the demanding rate and background conditions, the CSC are situated in the innermost plane covering the pseudorapidity range 2 - 2.7.

In the barrel region are used *Resistive Plate Chambers* (RPCs) and in the end-caps *Thin Gap Chambers* (TGCs). Additionally, these chambers operates as the trigger chambers for the muon spectrometer. RPCs and TGCs provide bunch crossing identification, well-defined $p_T$ thresholds and measure the muon coordinate in the direction orthogonal to that determined by the precision-tracking chambers.

## 2.3 Magnets

Strong magnetic field is very important for ATLAS as it is used to bend the tracks of charged particles from which information on their momenta ca be obtained. There are two magnetic systems that generate the magnetic field.

The solenoid magnet is located between the Inner Detector and the calorimeters. It provides 2T axial magnetic field for the inner detector and it is aligned with the beam axis.

The other system is composed of the toroid magnets and as well as the muon chambers

it is situated on the perimeter of the whole ATLAS detector. The barrel toroid consist of 8 coils with air cores and they are designed to provide magnetic field of 0.5 T. The end-cap toroids are essentially large cryostats and should provide a magnetic field of 1 T.

## 2.4 Trigger and Data Acquisition

The amount of data delivered by the LHC is enormous and it is impossible and unnecessary to store all data from every event. Therefore it is desirable to choose only the "interesting" ones. For this purpose ATLAS employs a three level trigger system. This is a very challenging task as the nominal bunch separation is 25 ns – the next bunch crossing happens before the products of the collisions from the previous crossing are able to reach the edge of the detector.

The LVL1 trigger needs about 2.5 μs to decide whether to sent the information about the event to LVL2 trigger or to the discard it. Then the information is passed to the High-level trigger. The output rate of the L1 trigger is 75 kHz, it is limited by the hardware. The input collision rate is about O(20 – 40) MHz.

*The High-level trigger* (HLT) is composed of *Level 2* (LVL2) and *Event Filter* (EF). Both are software trigger systems that run on a large processor farm adjacent to the ATLAS experimental cavern. This prevent any unnecessary delays from signal transport. Basically the LVL1 trigger selects so called *Regions of Interest* (RoI) and within these RoI the LVL2 uses full granularity information from the detectors. They RoI in general account for 2–6% of the total detector volume. The LVL2 uses fast algorithms and simplified selections to reduce the trigger rate down to ∼3.5 kHz. The LVL2 trigger (but not LVL1) also uses information from the Inner Detector to perform fast tracking. The processing of one event takes on average 40 ms.

The events accepted by the LVL2 trigger are passed to the *Event Builder* that assembles all the event fragments and passes the full event information to the last stage of the trigger selection: the Event Filter. Because it has access to the full detector information and also enough time for execution, the EF runs almost the same algorithms as used during off-line reconstruction and also the object selection is very similar to the one used off-line. The EF reduces the output rate to 300–400 Hz while spending on average 4 s on every event. The events that pass the trigger selection are written to the disk for reconstruction and analysis. The average size of the event from proton-proton collisions is approximately 1.3 MB.

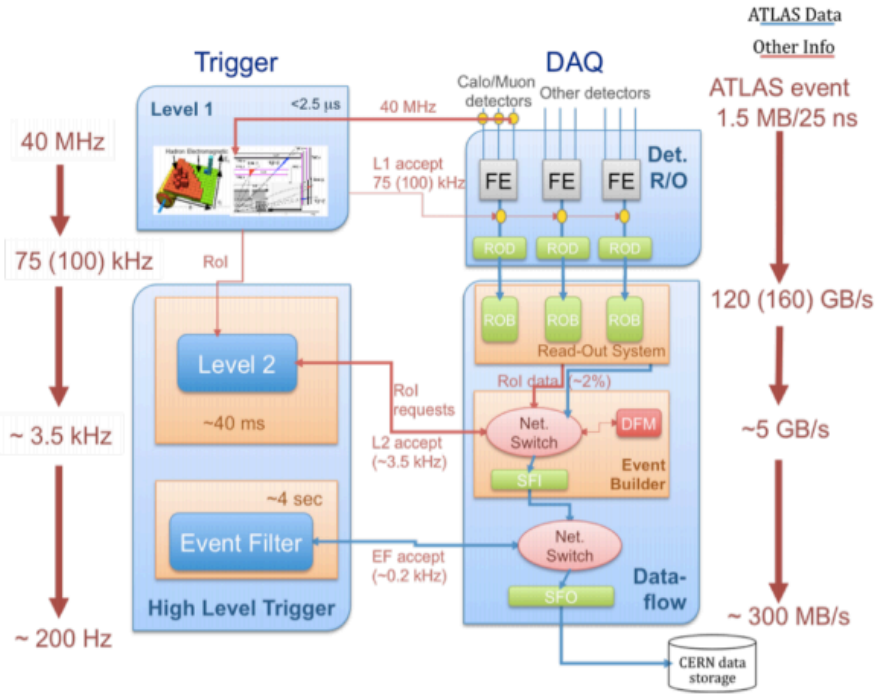


Figure 7: A schematic of the ATLAS Trigger Systems together with the Data Acquisition System of the detector combined with the readout systems [Trig].

# 3 Quarkonia and their role in the history of physics

## 3.1 From resonances to QCD

In 1932 the existence of neutron, the second constituent of atomic nucleus, was proved and it became obvious that electromagnetic force is too weak to keep the nucleons together. Next year Fermi proposed his theory of $\beta-$decay, which he formulated using the means of *relativistic quantum field theory*. Fermi theory represents a first decisive step towards very successful theory of *Electroweak interactions*. But it took another forty years to find an official explanation based on similar principles for strong forces that are (not only) binding the nucleons together in theory called *Quantum Chromodynamics* (QCD). QCD is also formulated within a language of the field theory and it was able to explain dynamics of nuclear forces as well as many other phenomenons that led to discovery of constituents inside some particles called hadrons.

Between 1930's and 1960's many discoveries of new particles there have been made. Many particles were identified in cosmic rays, others were produced in laboratories. But the meaningful way of classification of the growing particle zoo had not been successfully solved until 1964 when the quark model was introduced. Crucial step taken towards the quark model represents a discovery of the first resonance.

At that time most of the known particles have lifetime $\tau$ longer then $10^{-12}$s. These particles could be observed directly in bubble chambers or other detectors. But how to detect the ones with shorter lifetimes? Direct observation of such states, called resonances, is mostly impossible so their existence must be confirmed by other means.

The existence of resonance was first indicated in 1952 [QCD] by Fermi and his group. A resonance is in fact a peak located around a certain energy. Such increase can be found in dependencies of differential cross sections of scattering experiments on energy or in invariant mass distributions of decays, which final states consisting of two or three particles. The beam of $\pi^+$, used by Fermi, provided only very limited energy spectrum which disallowed him from discovery of the first resonance.

In 1954 at Carnegie Institute of Technology, several groups used a $\pi^-$ beam of 450 MeV to explore dependency of $\sigma(\pi^- p \to \pi^- p)$ on energy. Because of the small intensity of their beam they were able to see evident peak only in $\pi^- p$ channel. This resonance was called $\Delta^0$ and it is the first baryon resonance discovered (see figure 8). Hence it provided an evidence that the isospin invariance is valid for interactions of pions and nucleons. Later was $\Delta$ observed in all $\pi N$ channels which implied that it has isospin of $3/2$. It is a very nice coincidence that the first resonance family ever observed played later an important role in improvement of the so called *quark model* because it manifests the need for concept called

*colour*.

The hunt for more resonances began and soon after many more were really discovered for example: $\omega, \rho, \eta$ or $\Sigma^{*\pm}$. The first meson resonance $K^{*-}$ was observed in 1961 [Kstar]. But one of them called $\phi$ [Phi] was particularly interesting. At that time, there was no no obvious reason why decay channel $\phi \to \pi^+ + \pi^- + \pi^0$ should be suppressed with respect to $\phi \to K^+ + K^-$. On the contrary, the decay on three pions should be according to kinematics preferred before the kaon channel. This puzzling phenomenon was several years later successfully explained by the quark model.

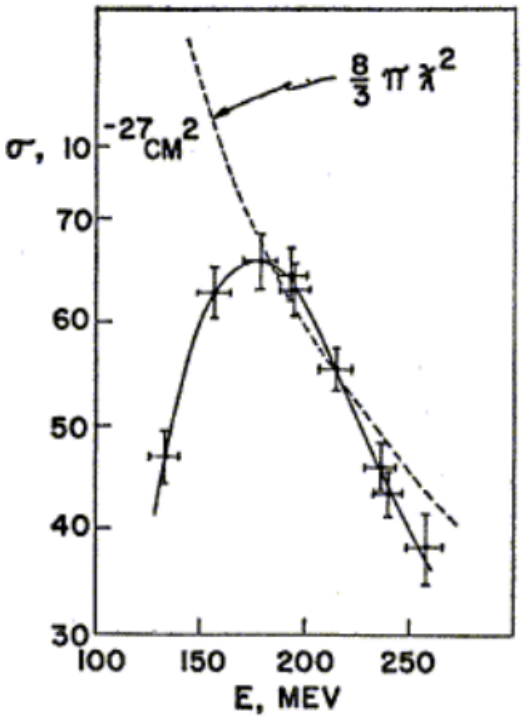


Figure 8: The $\pi^- p$ cross-section increase was the first experimental proof of the baryon resonance $\Delta_0$. Picture was taken from [Delta].

Of course in parallel with experimental searches for new particles the theorists were persistently making attempts not only to explain the steadily growing number of particles, but some of theirs peculiar properties too. In the beginning of this chapter I have mentioned the field theory postulated by Fermi in 1932 which he used to explain the $\beta$-decay of neutron. Next year young physicist Hideki Yukawa postulated that recently discovered new force (now called strong) is mediated by the massive particles and he revealed the relation

between the short range of the force ($10^{-15}$ m) and the mass of these particles.

He wrote it down in the form of potential corresponding to the exchange of mediating particle with the mass $m$

$$U(r) = -\frac{g}{4\pi r} e^{-\frac{r}{R}}. \tag{7}$$

From the relation $R = \hbar/mc \approx 1.4$ fm can be calculated mass of these particles $m \approx 140$ MeV.

This potential can be derived from Klein-Gordon equation

$$\frac{1}{c^2}\frac{\partial^2\psi}{\partial t^2} = \nabla^2\psi - \frac{m^2c^2}{\hbar^2}\psi. \tag{8}$$

If we look for solution of static approximation then the problem becomes spherically symmetric

$$\nabla^2 U(r) = \frac{1}{r^2}\frac{\partial}{\partial r}\left(r^2\frac{\partial U}{\partial r}\right) = \frac{m^2c^2}{\hbar^2}U(r). \tag{9}$$

After the integration over $r > 0$ we get the potential in the form of equation 7. In this equation the $g$ variable is equivalent to the charge $Q$ in electromagnetism and it can be referred as *strong charge*.

Yukawa was pointing in the right direction, but his potential had still some flaws. It was not charge invariant which was a discrepancy with later measurements according to which the force acting between proton and neutron has the same strength as between the proton and proton or neutron and neutron. Charge invariance in combination with almost the same masses of both nucleons led to formulation of the concept called isotopic spin (isospin). So it seemed natural to treat neutron and proton as two states of one particle. The isospin of nucleons was set to be $1/2$. Then neutron and proton were associated with different projection of isospin $p = |1/2, 1/2\rangle$ and $n = |1/2, -1/2\rangle$. Yukawa potential also provides no information on the spin of the mediating particles. Nevertheless, Hideki Yukawa contributed significantly, not only with this potential, and was in 1949 awarded the Nobel prize for his theoretical work on nuclear forces.

Yukawa's particles (named *pions*) were identified in cosmic rays in 1947 by Latters and coll. (for more information see [Pi]) which really have mass around 140 MeV and spin 0. In fact the discovery of these conjectured particles had been announced one year earlier because they had been mistaken for other particles called *muons*. But the penetrating effect of muons coming from cosmic rays soon excluded them from representing the quanta of strong force.

The Yukawa's concept was broadened by Kemmer in [Kem] who made corrections to the

missing charge invariance and his solution already in terms of field theory looked like

$$H_{int} = g\bar{\psi}(\tau_1\phi_1 + \tau_2\phi_2 + \tau_3\phi_3)\psi = g\bar{\psi}\vec{\tau}\psi\vec{\phi}, \tag{10}$$

where $\tau_{1-3}$ are Pauli matrices, $\phi_{1-3}$ the neutral scalar fields and $\psi$ stands for

$$\psi = \begin{pmatrix} \psi_p \\ \psi_n \end{pmatrix}.$$

The equation 10 differs significantly from 7 in the third term $\phi_3$, added by Kemmer, which stands for a neutral meson field of the same mass as the charged fields. That in fact means that he introduced new particle $\pi^0$ and by this he assured that the equation 10 is invariant under a simultaneous rotation of the nuclear doublet and meson triplet in the isospin space. Now we know that the true nature of the strong force seems to be much more complex and with other "particles" playing the role of mediators.

Pions were also final products of other particles decays discovered in 1947 decays. These particles are now called *kaons* and they demonstrate a very peculiar quality called strangeness. Kaons were produced in strong interactions but they decayed much slower than expected and with no obvious reason for it. Hence the decay rates of some channels were much smaller than expected. Gell-Mann solved this problem by assigning the particles into isospin triplet which forbid them to proceed through some channels in which the isospin invariance did not hold. For example Gell-Mann predicted that $\pi^-(-1) + p(1/2) \to K^+(1/2) + \Sigma^-(-1)$ (numbers in brackets are assigned third components of isospin) is preferred before $\pi^-(-1) + p(1/2) \to K^-(-1/2) + \Sigma^+(1)$ where the third component of isospin is not conserved.

Theorist were not fully satisfied with such phenomenological explanations and went further to look for a deeper reason of kaons strange behaviour. Gell-Mann (but he was not the first one) also realized that if he added a new quantum number (later called strangeness) which would be conserved in strong and violated in weak interactions, he would ended up with the correct predictions. He introduced so called Gell-Mann-Nishijima relation

$$Q = T_3 + \frac{Y}{2} = T_3 + \frac{B+S}{2}, \tag{11}$$

where $T_3$ is third component of isospin, $Y$ stands for *hypercharge* which is sum of the baryon number $B$ and strangeness $S$. The formula 11 does not hold any special restrictions on strong decays. Strangeness is in fact only a shift in conservation of $T_3$ and $Q$. However it led to formulation of so called unitary symmetry and was explained by a quark model.

Theoretical physicists were trying very hard to connect all peculiar dots with a right the-

Figure 9: Using recently improved photographic emulsion the physicist Cecil F. Powel observed decays of charge pions $\pi \rightarrow \mu \rightarrow e$ [Pi]. In 1950 was Powel awarded by the Noble prize: "For his development of the photographic method of studying nuclear processes and his discoveries regarding mesons made with this method".

ory. The first important line was drawn by Robert Mills and Chen Ning Yang in 1954 when they published an article called *Conservation of isotopic spin and Isotopic Invariance* [Y-M] describing the isotopic invariance in the terms of field theory. They took inspiration from the very successful field theory of *Quantum electrodynamics* (QED), but QED is build upon a U(1) symmetry, which is an Abelian group (also called commutative group). On the contrary Yang and Mills formulated their theory within the SU(2) group which is non-commutative. It took another 10 years to fully appreciate their insight.

Physicists also started to realize that it is improbable that all particles would be *elementary* – not bound states of other particles. This fact was firstly pointed out by Fermi and Yang in their article *Are mesons elementary particles?* [Mesons]

> "We assume that the $\pi$-meson is a pair of nucleon and anti-nucleon bound in this way. Since the mass of the $\pi$-meson is much smaller than twice the mass

> of a nucleon, it is necessary to assume that the binding energy is so great that its mass equivalent is equal to the difference between twice the mass of the nucleon and the mass of the meson."

Of course the assumption that nucleons are elementary proved to be wrong, moreover their suggestions have never been fully elaborated into self-standing theory. Just only the assumption that other particles can be bound states of others turned out to be very fruitful.

The breakthrough was an article by Yval Ne'eman published in 1961 [Ne] who has built his theory straightly demanding the gauge invariance. Which is obvious from his abstract

> "A representation for the baryons and bosons is suggested, based on the Lie algebra of the 3-dimensional traceless matrices. This enables us to generate the strong interactions from a gauge invariance principle, involving 8 vector bosons. Some connections with the electromagnetic and weak interactions are further discussed."

It implies that Ne'eman firstly chose the underlying SU(3) symmetry and gauge invariance and then he got the forces acting between particles (in his theory the role of mediating particles were played by eight vector mesons). On the other hand he continued in attempts to identify already known particles with his SU(3) triplets. In the end of the article [Ne] can be also found a very nice example of turbulent development of theoretical concepts in the beginning of 1960's.

> "Shortly after the present paper was written, a further version, utilizing the 8-representation for baryons, as in this paper, reached us in a preprint by Prof. M. Gell-Mann."

Gell-Mann was the first one who suggested to abandon the attempts of finding the right particles that are really elementary. He worked only with "abstract" SU(3) group and its representations. In the eight chapter of his paper called *The "eightfold way"* discussing the *Symmetries of baryons and mesons* he clearly suggested that: "unitary symmetry may be applied to the baryons in a more appealing way if we abandon the connection with the symmetrical Sakata model and treat unitary symmetry in the abstract. (An abstract approach is, of course, required if there are no elementary baryons and mesons.)" [8-way]. Sakata model was in fact a modification of Fermi-Yang model. Shoichi Sakata only added to elementary nucleons $\Lambda$, which allowed him to compose strange particles. He described this logical procedure in a very short article: *On a composite model for the new particles* [Sakata]. Even though, Gell-Mann elaborated previous chapters of [8-way] in terms of Sakata model, that is according to our present knowledge wrong, he built the foundations of quark model:

> "We consider a three-dimensional representation of the unitary spin algebra (note: the commutation rules for total unitary spin $F_i$ was defined by relation $[F_i, F_j] = if_{ijk}F_k$) or of the group SU(3) that is generated by the algebra. It is the representation to which $b$ belongs (that is, $e$,$p$, and $\Lambda$) and we may denote it by the symbol $\mathbf{3}$. The antiparticles $\bar{b}$ belong to the conjugate representation $\mathbf{3}^*$, which is inequivalent to $\mathbf{3}$. We have then taken the direct product $\mathbf{3} \times \mathbf{3}^*$ and found it to be given by the rule
>
> $$\mathbf{3} \times \mathbf{3}^* = \mathbf{8} + \mathbf{1}$$
>
> where $\mathbf{8}$ is the octet representation and $\mathbf{1}$ the singlet representation of unitary spin. Each of these is its own conjugate; that is a situation that occurs only when the dimension is the cube of an integer."

At this place should be noted that "×" and "+" in this case denotes *direct* product and sum which is easy to tell apart from the "classical" multiplication and addition. In the last equation, it is suggested that meson can occupy one of the representations $\mathbf{1}$ or $\mathbf{8}$. All baryons could be assigned to the representations that are on the l.h.s

$$\mathbf{3} \times \mathbf{3} \times \mathbf{3}^* = \mathbf{15} + \mathbf{6}^* + \mathbf{3} + \mathbf{3}. \quad (12)$$

In [8-way] Gell-Mann assumed that the triplets of basic fields are abstract objects:

> "There is no longer any reason for the baryons to belong to the $\mathbf{3}$ representation or the other spinor representations of the group SU(3); the various irreducible spinor representations are those obtained by reducing direct products like $\mathbf{3} \times \mathbf{3} \times \mathbf{3}^*$, $\mathbf{3} \times \mathbf{3} \times \mathbf{3} \times \mathbf{3}^* \times \mathbf{3}^*$, etc. Instead, the baryons may belong, like the mesons, to representations such as $\mathbf{8}$ or $\mathbf{1}$ obtained by reducing the direct products of equal numbers of $\mathbf{3}$'s and $\mathbf{3}^*$'s. It is then natural to assign the stable and metastable baryons $N$, $\lambda$, $\Sigma$, and $\Xi$ to an octet, degenerate in the limit of unitary symmetry."

In this short passage Gell-Mann very indirectly submitted his proposition of other baryons representations, that rose from relation

$$\mathbf{3} \times \mathbf{3} \times \mathbf{3} = \mathbf{10} + \mathbf{8} + \mathbf{8} + \mathbf{1}. \quad (13)$$

But the equation 13 was not in such explicit form written in the whole article.

## 3.2 Quark model

In the beginning I would like to summarize the most acute problems *yet to be solved* in particle physics just before the birth of quark model:

- Concept of strangeness was known but the underlying reason was still missing.
- Puzzling decay rates of $\phi$ resonance remained still unexplained.
- SU(3) group seemed to be the right building block for particle zoo classification, but it was not known which representations were actually demonstrated in nature.

In 1962 at a conference in Geneva were announced two more discoveries of resonances $\Xi^{*-}(1530)$ and $\Xi^{*}(1530)$. This two particles very well corresponded with the baryons from decuplet that existence was predicted in models of Ne'eman and Gell-Mann. Immediately after the lecture Gell-Mann suggested the existence of the last baryon $\Omega^-$ missing in the decuplet, that came from equation 13, and its expected mass (see figure 11). The last piece from the decuplet puzzle was discovered in 1964 (see figure 10) and the Eightfold way was proven to be the right concept.

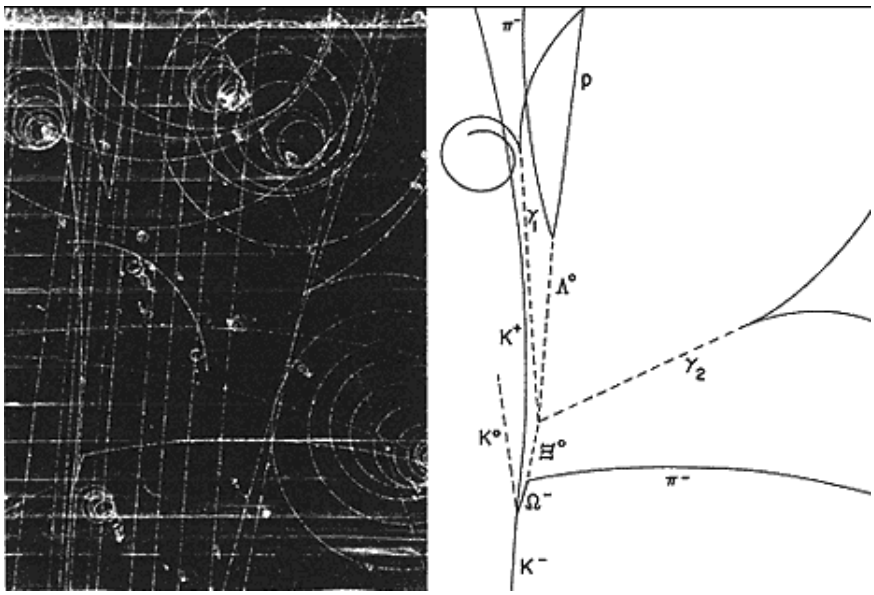


Figure 10: Discovery of $\Omega^-$ [Omega]. Incoming $K^-$ is interacting with proton in liquid nitrogen. Products of the collision are $K^0K^+\Omega^-$ particles that also subsequently decay.

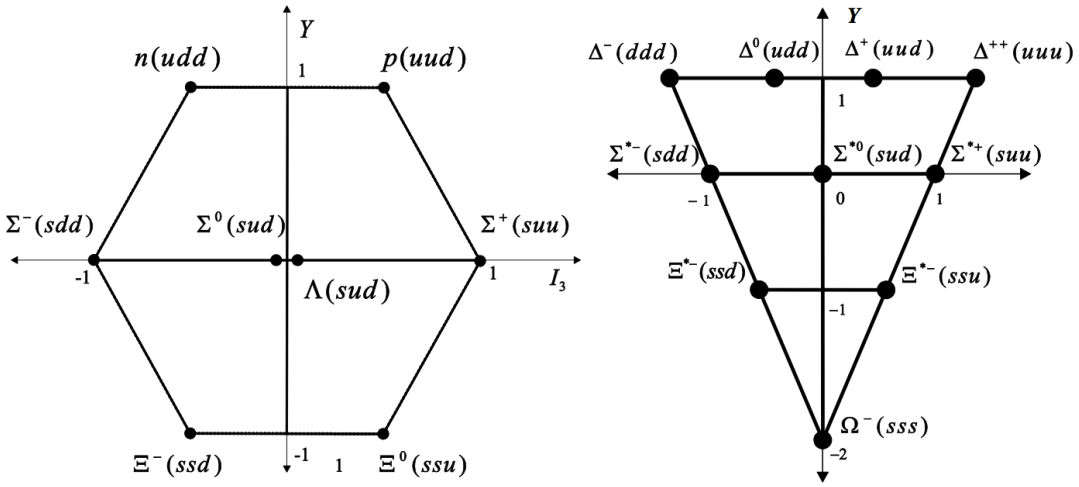


Figure 11: Example of baryon octet with spin and parity $J^P = 1/2^+$ (left) and baryon decuplet $J^P = 3/2^+$ (right).

Just one day after the discovery of $\Omega^-$ on $1^{st}$ January 1964 another paper called *A schematic model of baryons and mesons* [Quarks] by Murray Gell-Mann has been published. In this short article he suggested, with absolutely no hesitation, that fundamental triplets consist of new objects with fractional charge, spin 1/2 and baryon number of 1/3. Gell-Mann named these objects *quarks up*, *down* and *strange*. It is interesting that quark is a meaningless word used by James Joyce in his book Finnegan's wake ("Three quarks for Muster Mark!") [Quarks]. From [Quarks]

> "Baryons can now be constructed from quarks by using the combinations $(qqq)$, $(qqqq\bar{q})$, etc., while mesons are made out of $(q\bar{q})$, $(qq\bar{q}\bar{q})$, etc. It is assuming that the lowest baryon configuration $(qqq)$ gives just the representations **1**, **8** and **10** that have been observed, while the lowest meson configuration $(q\bar{q})$ similarly gives just **1** and **8**."

is obvious that Gell-Mann theory was not yet perfect but at that time the concept of colour, which excluded quarks combinations of higher order then $(qqq)$ for baryons and $(q\bar{q})$ for mesons, was yet to be found. On the other hand all important aspects of quark model were introduced (for complete set of quarks properties see table 2). Basically for this and also for prediction of $\Omega^-$ was Murray Gell-Mann in 1969 awarded Nobel prize. It was only a shame that Yval Ne'eman's contribution remained unrecognised, even if he was ready to present the same results as Gell-Mann. Yval Ne'eman was not the only whose contribution

was not sufficiently appreciated. Just three weeks later a young postdoc George Zweig, inspired by Ne'eman's article [Ne], came up with a complete set of calculations that could be done within a quark model (of course Zweig did not name basic triplets and anti-triplets constituents as quarks) in his preprint called *An SU(3) model for strong interaction symmetry and its breaking* ( see [Zweig]). On the contrary Gell-Mann's paper was only a very short note where he described what could be done within his model and presented the expressions for electromagnetic and weak currents. What is even more fascinating that Zweig's article has been revoked by publishers. In this masterpiece he also introduced so called Zweig or OZI rule (Susumu Okubo and Jugoro Iizuka suggested independently on each other the same rule). They divided all processes into two groups

1. Allowed processes are the ones with connected lines in the left to right direction.

2. The forbidden processes are the ones with disconnected lines.

Allowed processes always dominates over the suppressed ones but the rates depends also on other factors. For a demonstration of such rule see figure 12.

The quarks carrie so called *flavour* charge *up*, *down* and *strange* (see table 2). As the quarks are fermions it became soon obvious that in fact they exist in 6 different states. So the SU(3) flavour symmetry should be broadened to SU(6) flavour-spin symmetry

$$\mathbf{6} \times \mathbf{6} \times \mathbf{6} = \mathbf{56} + \mathbf{70} + \mathbf{70} + \mathbf{20}. \tag{14}$$

Accordig to the quark model, there are 56 baryons it is logical to choose the multiplet **56** which has the right number of states but it is also fully symmetric. It means that the wave function is symmetric under any permutation of quarks.

Similarly for mesons the decomposition gives

$$\mathbf{6} \times \mathbf{6}^* = \mathbf{35} + \mathbf{1}. \tag{15}$$

## 3.3 Partons and colour on the scene

After the announcement of quark model successes, the experimental hunt for particles with fractional charge began. At that time there was not known reason why the free quarks should not exist in nature. But such quarks have been never detected and now we know that it was because of principle called *quantum confinement*. The confinement is a consequence of so called *asymptotic freedom* in the strong interactions that was discovered by

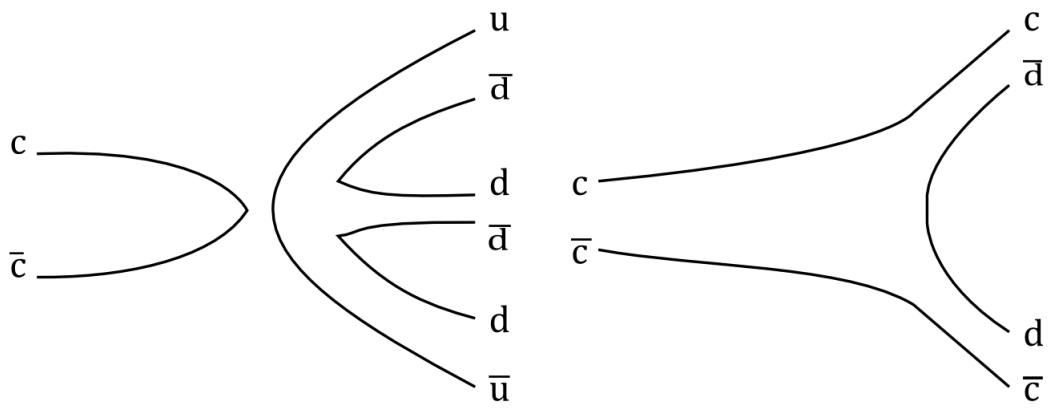


Figure 12: Process on the right is according to Zweig (OZI) rule allowed and the process pictured on the left is Zweig forbidden.

David Gross, David Politzer and Frank Wilczek in [Asymptotic] and [Asymptotic2]. Asymptotic freedom is a property that causes bonds between particles to become asymptotically weaker as energy increases and distances decreases. Hence it means that the other side of the asymptotic freedom is confinement. As the force acting between colour charges *increases* with distance, it causes that quarks and gluons can never be liberated from hadrons. The importance and uniqueness of such principle can be demonstrated on fact that all previously named physicist were awarded the 2004 Nobel Prize in Physics.

The experiments with inelastic scattering an SLAC have proven to be very fruitful [Rior]. The first experiment that used electrons with energies of 20 MeV to bombard protons, gave no evidence that protons consist of quarks. It was due to the small electron energy which resulted in *elastic* scattering. The next experiment was already working in *inelastic* region and performed by combined group of physicists from MIT and SLAC. In 1967 they were measuring electrons that rebounded from protons at angle of 6°. For each given values of energy $E$ and angle $\phi$ they measured energies ranging from elastic electron-proton scattering at the highest $E'$ down to the deep inelastic scattering at a few GeV. The experimental set-up was not the best fitted because the electrons, with energy $E$, were passing through liquid hydrogen or later deuterium. Electrons that rebounded at 6° into the acceptance of the 20 GeV spectrometer were momentum analysed. Those with a scattered energy, that fell into a range of about $\pm 2\%$ around a central value E', were directed in a group of particle detectors that distinguished electrons from a background consisting mostly of pions. Due to the experimental environment, a lot of radiative corrections (electrons radiate photons as they

recoil or pass through material) had to be calculated before the official verdict could have been published. Even after that, the counting rates in deep inelastic region remained much higher then expected. Also the momentum transfer to the proton $Q^2 = 2EE'(1 - cos\phi)$ decreased much more slowly in case of the deep inelastic scattering than for the elastic one (see figure 13). This could be interpreted as electrons hitting some kind of hard components inside the proton. However there were several possible interpretations of the inelastic data that had to be excluded before the absolute confirmation of proton constituents discovery.

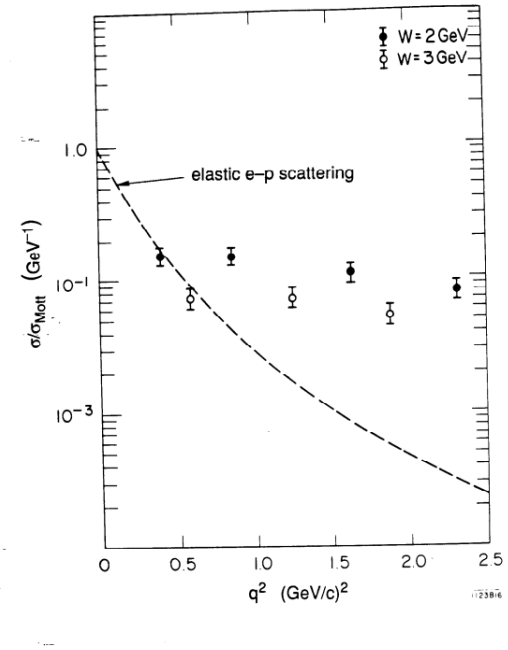


Figure 13: Cross-sections for inelastic electron-proton scattering measured at 6° by combined group of MIT and SLAC. It was normalized by those expected for Mott scattering from a point proton. The data points are given for two values of $W$ which is the invariant mass of the unobserved final-state hadrons. (Figure is from [Rior].)

In 1968 Henry W. Kendall plotted the dependence of $\nu W_2$ where $\nu = E - E'$ on $\nu/Q^2$. The $W_2$ is mostly denoted as proton *structure function*. If we take the first Born approximation, it means that the process of electron-proton scattering is mediated by one photon, then two structure functions $W_1$ and $W_2$ are needed. The cross-section of such process have a form

$$\sigma(E, E', \phi) = \frac{4e^2E'^2}{Q^4}\left[W_2(\nu, Q^2)\cos^2\frac{\phi}{2} + 2W_1(\nu, Q^2)\sin^2\frac{\phi}{2}\right], \tag{16}$$

where $W_2$ factor is dominant at small angles, while $W_1$ at large angles. Kendall extracted $W_2$ from the MIT-SLAC experiment data. According to an earlier prediction of James Bjorken the data appeared to fell along a curve $F_2 = \nu W_2$ which is a function of $\nu/Q^2$ and not of $\nu$ and $Q^2$ independently (see figure 14). This *scaling factor* was interpreted by Richard Feynman as a consequence of existence of so called *partons*. Feynman did not specified any quantum numbers of partons, they resulted merely from a more or less phenomenological studies, that can be found in [Feyn]:

> "It is the purpose of this paper to make suggestions as to how these cross sections might behave so that significant quantities can be extracted from data taken at different energies. These suggestions arose in theoretical studies from several directions and do not represent the result of consideration of any one model. An extraction of those features which relativity and quantum mechanics and some empirical facts' imply almost independently of a model. I have difficulty in writing this note because it is not in the nature of a deductive paper, but is the result of an induction. I am more sure of the conclusions than of any single argument which suggested them to me for they have an internal consistency which surprises me and exceeds the consistency of my deductive arguments which hinted at their existence."

According to this model partons are only a point like constituents of proton from which the high-energy electrons rebound elastically. He recognized that the universal function $F_2$ was the momentum distribution of the partons, weighted by the squares of their charges, when plotted versus a $x = Q^2/(2M\nu)$, where $M$ stands for the proton mass. The $x$ actually represents the fraction of proton momentum carried by parton in which the electron is at rest and the proton is speeding towards it, which Feynman named *infinite momentum frame*. The spin of partons can be determined from relation

$$R = \frac{\sigma_L}{\sigma_R} = \frac{W_2}{W_1}\left(1 + \frac{\nu^2}{Q^2}\right) - 1, \tag{17}$$

no indent where $\sigma_L$, respectively $\sigma_T$, stands for cross section for *longitudinally*, respectively *transversally* polarized photons.

By 1973, enough evidence has been collected to conclude that proton has an internal structure. It was confirmed in four different kinds of high-energy scattering experiments: electron-nucleon, neutrino-nucleon, electron-positron and proton-proton, in which three different forces were involved: the electromagnetic, the weak and the strong nuclear force. There was also fairly solid evidence that these constituents had the quantum numbers cor-

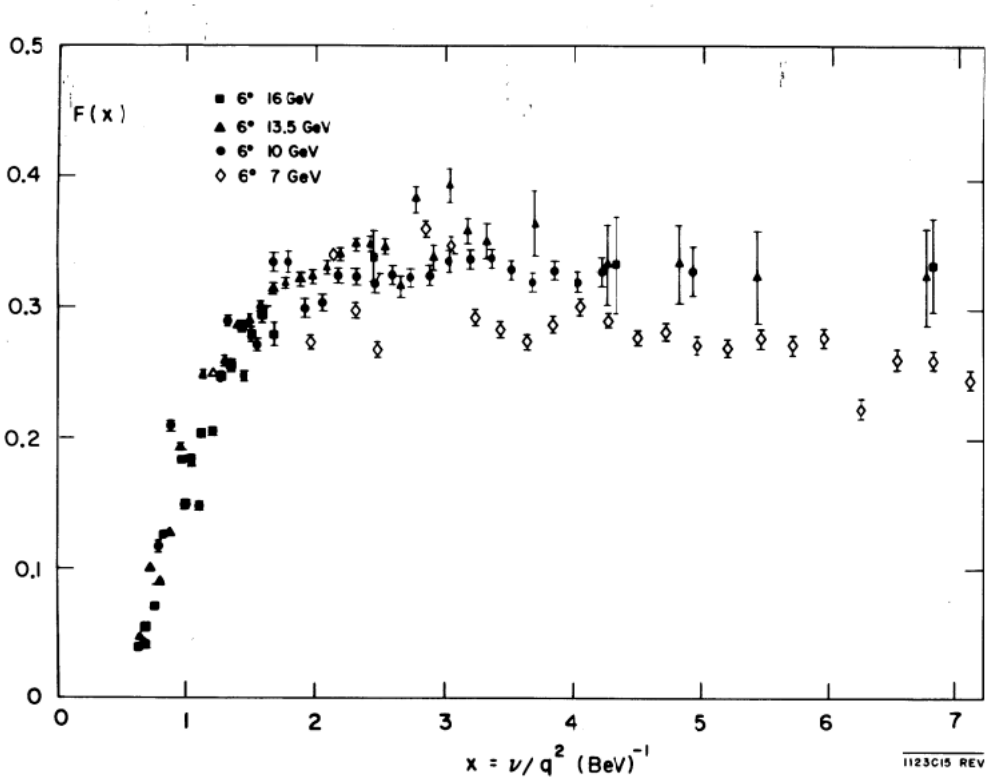


Figure 14: Values of the proton structure function $F_2$ obtained from MIT-SLAC experiment. As anticipated by Bjorken, the data appeared to be a universal function of the ratio $\nu/q^2$ and even more when the low-$q^2$ data at E = 7 GeV were excluded from the sample. Figure was taken from [Rior].

responding to quarks. But free quarks were never found despite continuing efforts.

The absence of free quarks was only one of the problems that the quark model had to face. The other was that baryons were assigned into *symmetric* multiplet but quarks as fermions cannot have symmetrical wave function if we interchange all their characteristics. There was also no sign of particles which should correspond to states like $(qq\bar{q}\bar{q})$ or $(qqqq\bar{q})$.

The first promising suggestion was made by Oscar Greenberg in [Para]. According to [Para], parafermions are like fermions with rank three:

> "Now we return to the question of placing three spin-1/2; quarks in $s$ states in the baryon 56. This can be done if the quarks are parafermions of order $P = 3$. This suggestion is the main new idea of this article."

In 1965, just six month later an article by Yoichiro Nambu and Moo-Young Han was pub-

lished, in which they suggested that there are three triplets of quarks. That each quark exist in different colour and the particles, which can be observed, are colourless states, or white combinations, of these colours. This small modification solved the problem of quark model and in 2008 Nambu was awarded the Nobel prize. The concept of colour was finally established in paper by Bardeen, Fritzch and Gell-Mann [Colour]:

> "An equivalent description, easier to follow, involves introducing nine types of quarks, that is, the usual three types in each of three "colors," say red, white, and blue. The restriction is then imposed that all physical states and all observable quantities like the currents be singlets with respect to the SU(3) of color (i.e., the symmetry that manipulates the color index). Again, the quarks are fictious. Let us refer to this type of statistics as "quark statistics."

This quotation also illustrates that Gell-Mann originally considered quarks only as mathematical concept, not as real constituents existing inside.

## 3.4 More quarks for Muster Mark

"Colourless rule" didn't exclude some of the the higher quark combinations like $(qq\bar{q}\bar{q})$. In this case, the most successful "puzzler" was again Nambu (even if similar results can be found in Greenberg's paper [Para]). In this proceeding, Nambu introduced eight gauge fields and he coupled them to the $SU_c(3)$ colour triplets. The exchange of gauge fields was responsible for super-strong interaction and so called *quark confinement*. The other important consequence was that the eight gauge bosons, that played the role of mediators, carried the colour charge. Nambu formulated his theory independently on others, he did not use the word quark. He wrote his theory in language of non-relativistic quantum mechanics but his ideas were later also transformed into *Quantum Chromodynamics*.

Very nice summary of Nambu's work can be found in [QCD] according to which the quark confinement follows from the basic assumption that the interaction is mediated by exchange of octet of coloured gauge bosons and has following properties

- The mass of free quarks is high enough to make free quarks unobservable.
- Forces acting between quarks are attractive only in colour singlet channels in which they have finite masses.
- In all other channels the forces are repelling, which makes them not observable.
- The force acting between $(q\bar{q})$ is twice as big as between $(qq)$.

In his paper named *Systematics of hadrons* (published in [Prel]) he described in semi-quantitative way potentials and bound energies of $(qq)$, $(q\bar{q})$ and $(qqq)$ combinations. The most interesting part is dedicated to calculations of states consisting of three triplets, altogether containing nine fermions

> "An important difference from the two–triplet case is that instead of charm gauge group U(1), we have the group SU(3)" (Note: Can be associated with $SU_c(3)$.). The charm gauge field $C$ must then be replaced by an octet of gauge fields $G_\mu$, $\mu$=1...,8, coupled to the infinitesimal SU(3)" generators (currents) $\lambda''_\mu$ of the triplets, with a strength $g$. For a system containing altogether N particles, the exchange of such fields between a pair then results in an interaction energy
>
> $$V_G = g^2 \sum_{n>m} \lambda''^{(n)}_\mu \cdot \lambda''^{(m)}_\mu = \frac{1}{2} g^2 \left[\sum_{n=1}^{N} \lambda''^{(n)}_\mu\right]\left[\sum_{m=1}^{N} \lambda''^{(m)}_\mu\right] - \frac{1}{2} g^2 \sum_{n=1}^{N} \lambda''^{(n)}_\mu \lambda''^{(n)}_\mu$$
> $$= -\frac{1}{2} g^2 [C_2 - N C_{20}]$$
>
> where $\lambda''^{(n)}_\mu$ refers to the n-th particle, $C_2$ is the quadratic Casimir operator of SU(3) and $C_{20} = 4/3$ is its value for a triplet representation D(1, 0) or D(0, 1)."

$C_2$ is in general for a representation $D(l_1, l_2)$ given by

$$C_2(l_1, l_2) = \frac{1}{3}(l_1^2 + l_1 l_2 + l_2^2) + (l_1 + l_2), \tag{18}$$

which implies that for SU(3)" $C_{20} = 4/3$. Nambu in his paper also introduces total energy

$$E = M + V_G = \left(M - \frac{1}{2} C_{20} g^2\right) N + \frac{1}{2} g^2 C_2, \tag{19}$$

where $M$ (M » 1 GeV) stands for so called common mass which denotes the mass of a free quark.

Bound states will have $V_G < 0$ and the lowest state will have $C_2 = 0$ which is singlet $D(0, 0)$. Now we have

$$E = N\left(M - \frac{1}{2} C_{20} g^2\right) = m = N\mu \tag{20}$$

where $m$ is a baryon mass. Nambu introduced in equation 20 variable $\mu$ which is a fraction of baryon mass.

$$E = \frac{1}{2}\mu N + \frac{1}{2} g^2 C_2 \tag{21}$$

In 1974 was found a new resonance simultaneously at SLAC (Stanford National Accelerator Laboratory) [Psi] and at BNL (Brookhaven Nationa Laboratory) [J] in the cross section of $e^+ + e^-$, respectively $p + Be$. The most interesting property of this resonance is very nicely illustrated at the end of the article [Psi]:

> "The $e^+e^-$–hadron cross section is presumed to go through the one-photon intermediate state with angular momentum, parity, and charge conjugation quantum numbers $J^{PC} = 1^{--}$. It is difficult to understand how, without involving new quantum numbers or selection rules, a resonance in this state which decays to hadrons could be so narrow."

The new resonance ended up with an exotic name $J/\psi$. Both research groups observed a very sharp peak at 3.1 GeV, hence at SPEAR other resonance $\psi'$ at 3.7 GeV was identified (see figure 16). The width that was measured by both experiments is mostly dominated by their resolutions (see figures 16). The total width was in fact much smaller and was determined from the leptonic branching ratios and the total reaction rate. The formula for cross section of $e^+e^- \to J/\psi \to e^+e^-$ can be deried from Breit-Wigner formula (in not relativistically invariant form)

$$\sigma(E) = \frac{4\pi\lambda^2(2J+1)}{2s_1+1)((2s_2+1)} \frac{\Gamma_{e^+e^-}^2/4}{[(E-E_R)^2+\Gamma^2/4]} \tag{22}$$

where $\lambda$ is a de Broglie wavelength of electron, $\Gamma$ is the total width (sum of all partial widths for every channel), $\Gamma_{e^+e^-}$ is partial width for process $J/\psi \to e^+e^-$, $s_1$ and $s_2$ are spins of the incident and target particles (in this case incident particles forming the resonant state), $J$ is the spin of a resonance $E$ is the CMS energy of colliding particles and $E_R$ is the resonance energy. To get the integrated cross section the $\sigma(E)$ has to be integrated over the energy $E$ and after inserting all numbers the result $\Gamma_{J/\psi} = 87$ keV is obtained. Other vector mesons resonances differ in several orders of magnitude, for example $\Gamma_\rho = 150$ MeV or $\Gamma_\omega = 8.4$ MeV. The second discovered resonance $\psi'$ (now denoted as $\psi(2S)$) has also very small width $\Gamma_{\psi'} = 280$ keV.

It was impossible to find good explanation in terms of known quark flavours $u$, $d$ and $s$. One more quark called *charm* (denoted as $c$) was needed. In fact, the existence of the fourth quark had been predicted some time earlier. The motivation came up mostly from an analogy with families of fermions but there were also other, deeper reasons for charm introduction. The so called *GIM* mechanism named after Sheldon Lee Glashow, John Iliopoulos and Luciano Maiani in [GIM] is clarified with the help of the fourth quark. The fourth quark was needed to explain the existence of the flavour changing neutral currents (FCNC)

suppression and to make clear why weak interactions changing strangeness by factor two are suppressed while this cannot be said about those, that change strangeness by one. The new quantum number charm (denoted $C$) is also like strangeness conserved in strong and electromagnetic interactions. It was postulated that these two new resonances consist of massive quark-anti-quark combination $c\bar{c}$, sometimes denoted as *charmonium*.

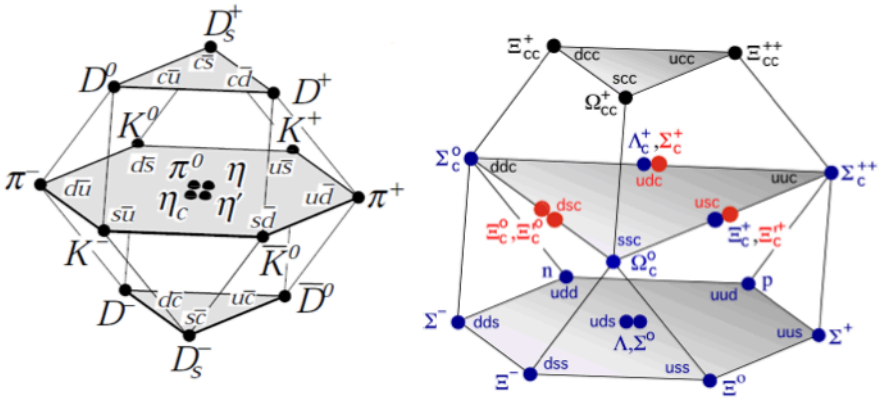


Figure 15: Examples of multiplets of particles consisting of $u$, $d$, $s$ and $c$ charmed mesons (left) and baryons (right) [PDG].

Since that time, to picture a particle multiplet one more axis for charm is needed, as it is illustrated in the figure 15. Later were observed higher excitation of $c\bar{c}$: $\psi(3S)$, $\psi(4S)$ and $\psi(5S)$. Other mesons that consist of only one charm quark and one from the original triplet $D$ were also soon discovered at SLAC and generically called D. The lightest D meson has mass of 1870 MeV [PDG] and for previously mentioned higher excitation it is possible to undergo decay $\psi(3S) \rightarrow D^+D^-$. For $J/\psi$ with mass of 3096 MeV and $\psi'$ with 3686 MeV, it is kinematically not possible. The significantly smaller width can be explained as consequence of possible decay patterns of $c\bar{c}$ only on $u$, $d$ and $s$ in Zweig suppressed channel (see again figure 12). Now I should switch from SU(3) to SU(4) group which (has some interesting consequences) but the most important fact is that the famous charge relation now have a form

$$Q = T_3 + \frac{Y + C}{2}. \tag{23}$$

In 1977 there were discovered resonances with similar patterns as $\psi$ family but with higher masses that can be attributed to a new quark. On Fermilab spectrometer was observed a new cascade of resonances called $\Upsilon$ (see [Upsilon]) in reactions $p + Be, Cu, Pt \rightarrow \mu^+ + \mu^- + anything$. The three observed states of $\Upsilon$: $\Upsilon(1S)$, $\Upsilon(2S)$ and $\Upsilon(3S)$ have masses between

| | Quark flavour | | | | | |
|---|---|---|---|---|---|---|
| Property | d | u | s | c | b | t |
| $m$ [MeV] | 4.1–5.7 | 1.7–3.1 | $100^{+30}_{-20}$ | $1.29^{+0.05}_{-0.11}$ GeV | $4.19^{+0.18}_{-0.06}$ GeV | 172.9±1.5 GeV |
| $Q$ | $-1/3$ | $+2/3$ | $-1/3$ | $+2/3$ | $-1/3$ | $+2/3$ |
| $I$ | $+1/2$ | $+1/2$ | 0 | 0 | 0 | 0 |
| $I_3$ | -1/2 | $+1/2$ | 0 | 0 | 0 | 0 |
| $S$ | 0 | 0 | $-1$ | 0 | 0 | 0 |
| $C$ | 0 | 0 | 0 | $+1$ | 0 | 0 |
| $B$ | 0 | 0 | 0 | 0 | $-1$ | 0 |
| $T$ | 0 | 0 | 0 | 0 | 0 | $+1$ |

Table 2: Summary of quarks quantum numbers where $m$ denotes mass, $Q$ electric charge, $I$ isospin, $I_3$ the $3^{rd}$ component of isospin, $S$ strangeness, $C$ charm , $B$ bottomness/beauty and $T$ topness. Taken from [PDG]

.

9.4 to 10.4 GeV (see [Upsilon] and [Upsilon2]). The fifth heavy quark called *bottom* and fifth quantum number denoted *bottomness* (or *beauty*) has been introduced. For these three upsilons states, it is not kinematically possible to decay on the lightest bottom mesons $B\bar{B}$. But there are three more resonances: $\Upsilon(4S)$, $\Upsilon(5S)$ and $\Upsilon(6S)$ which lie above the $B\bar{B}$ threshold.

The last and the heaviest quark that was needed to complete the quark family was experimentally discovered in 1995 at Fermilab and called *top* quark [Top]. This quark with mass of $172.9 \pm 1.5$ GeV (see also 2) is too heavy to form any bound ("topponium") state.

## 3.5 Quantum Chromodynamics

Quantum Chromodynamics (QCD) is a gauge field theory which is based on the SU(3) gauge groups. A gauge theory is a special type of field theory in which the Lagrangian is invariant under a group of local transformations. It describes the strong interaction which is a fundamental force acting between quarks and gluons. Gluons are the mediators of strong interaction in QCD. As I have already mentioned, QCD is a non-Abelian theory which implies the possibility of self-interaction of gluons. On the contrary, there is no self-interaction of photons in QED.

In would be the Zweig rule explained with the help of gluon exchange. For examples of Feynman diagrams of gluon-gluon interactions see figure 17. Gluons rise from combination of colour and anti-colour triplet and they belong to the octet.

$$\mathbf{3} \times \mathbf{3}^* = \mathbf{8} + \mathbf{1} \tag{24}$$

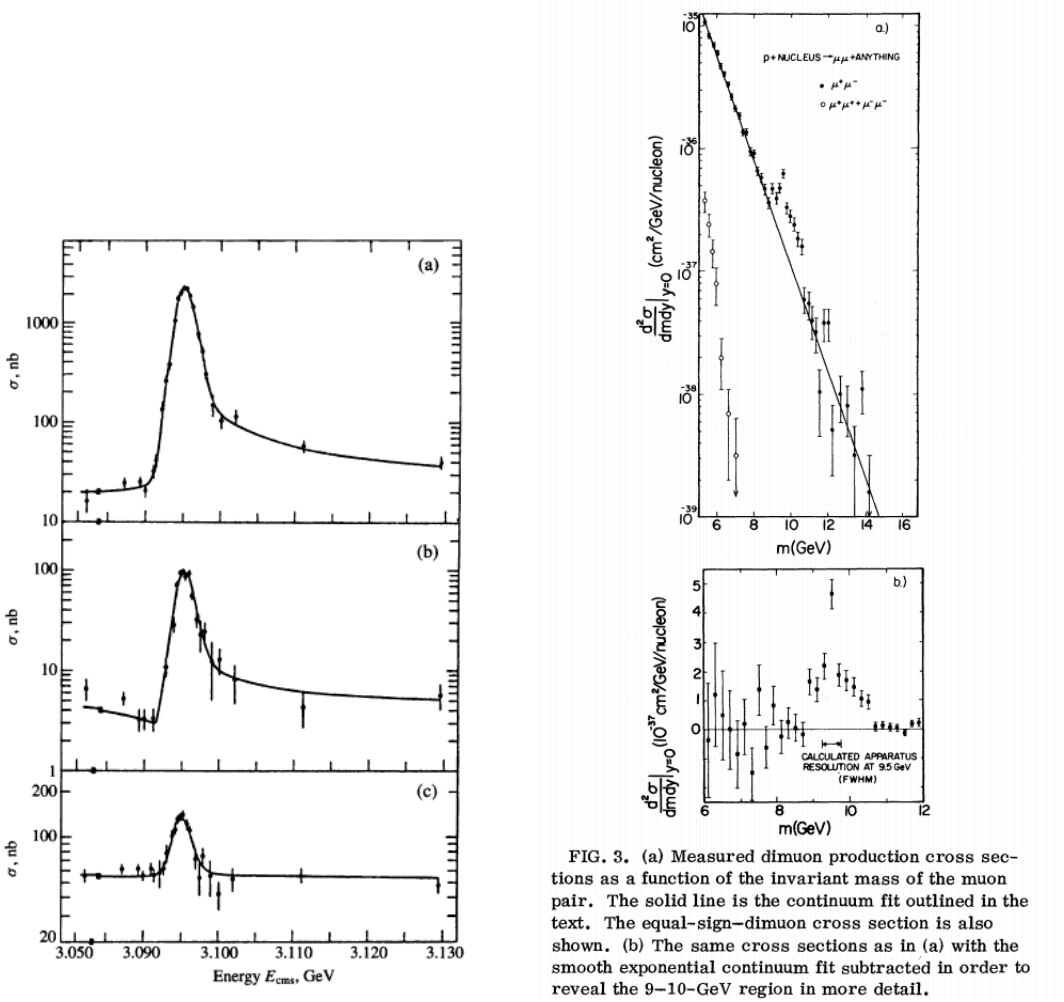


FIG. 3. (a) Measured dimuon production cross sections as a function of the invariant mass of the muon pair. The solid line is the continuum fit outlined in the text. The equal-sign–dimuon cross section is also shown. (b) The same cross sections as in (a) with the smooth exponential continuum fit subtracted in order to reveal the 9–10-GeV region in more detail.

Figure 16: Results from [Psi] presenting the $J/\psi$ resonance produced at SPEAR ring at SLAC (left). The first glimpse of $\Upsilon$ resonance from [Upsilon] (right).

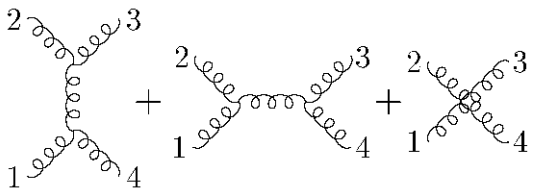


Figure 17: Gluon self-interaction diagrams.

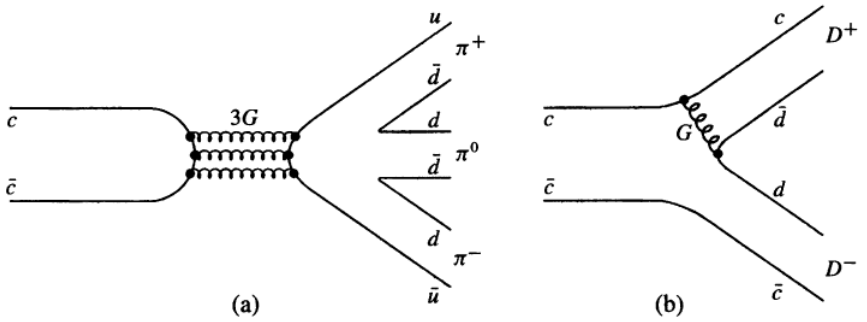


Figure 18: The example of Zweig rule applied to $J/\psi$ in QCD [Perkins].

Then the singlet state will have form

$$g_0 = \frac{1}{\sqrt{3}}(R\bar{R} + B\bar{B} + G\bar{G}) \tag{25}$$

where $R$ stands for *red*, $B$ for blue and $G$ for green an the rest for their anti-colours. In the singlet state the colour charges are completely neutralised which implies that this state does not interact with other quarks and that there are no gluon singlets. The octet of gluons can be constructed in a close analogy with the octet of mesons, only three flavour triplet must be interchanged for three colours. It also must be noted that in the case of gluons there is no analogue with particle isospin.

In figure 18 (b) for the kinematically forbidden decay $J/\psi \to D^+D^-$, one gluon exchange is sufficient to assure the transmission from $c$ to $\bar{d}$. In the case (a) of decay on three muons, there are at the beginning and at the end two almost separate colourless states, so at least two gluons are needed. But $J/\psi$ is a spin triplet which in analogy with the positronium (bound state of $e^-e^+$) must decay through an odd number of gluons and the lowest odd number for this case is three. The first process is mediated by so called *soft gluon*. This process is favoured by the QCD, but again forbidden by energy conservation. The other decay proceeds through exchange of triplet of *hard gluons*. They are called hard because the norm of their four-momentum is the square of the mass of the decaying resonance. The way to QCD has been paved, now it is time to summarize all important bits and pieces of information connected exclusively to QCD that were already revealed in this text and fully exploit them in the language of a field theory:

- QCD is a gauge field theory based on a SU(3) gauge group.

- It is similar to the QED but its non-Abelian (non-commutative) which results in gluon self-interaction.
- The structure demonstrates some interesting properties like asymptotic freedom and confinement of quarks which results in exclusive existence of colour singlets.

The Lagrangian density describing the interactions of quarks and gluons in QCD have a form

$$\mathcal{L} = -\frac{1}{4} G_{\nu\mu}^{(a)} G^{\nu\mu(a)} + \sum_q \overline{\psi_q^i} \left[ \gamma^\mu \left( iD_\mu \right)_{ij} - m\delta_{ij} \right] \psi_q^j + \mathcal{L}_{gauge} + \mathcal{L}_{ghost}, \tag{26}$$

where $\psi_q^i$ are three-component Dirac spinors of the quark fields with colour $i$ and flavour $q$. The interaction terms of the theory result from imposing local gauge invariance on the classical Lagrangian density for non-interacting quarks and gluons. $\mathcal{L}_{gauge}$ stands for the gauge fixing term and $\mathcal{L}_{ghost}$ is so called Faddeev-Popov ghost which must be introduced to guarantee the consistency of the quantization procedure, in particular the unitarity of the theory. In Feynman diagram calculations, ghosts behave as scalar particles, that couple to gauge bosons, but they appear only in propagators.The term

$$G_{\mu\nu}^{(a)} = \partial_\mu A_\nu^a - \partial_\nu A_\mu^a - g f_{abc} A_\mu^b A_\nu^c \tag{27}$$

represents the kinetic part of gluon fields that are responsible self-interaction of gluons via three- and four-point vertices, giving rise to the property of asymptotic freedom. $A_\nu^a$ stand for eight gluon fields. The covariant derivative

$$\left( D_\mu \right)_{ij} = \delta_{ij} \partial_\mu + ig \sum_a \frac{(\lambda^a)_{ij}}{2} A_\mu^a \tag{28}$$

where $f_{abc}$ are the structure constants that, with addition of the Gell-Mann matrices $\lambda$, satisfies the commutation relation $[\lambda_a, \lambda_b] = 2i f_{abc} \lambda_c$. All Feynman rules for QCD which can be found in Appendix A, can be derived from the Lagrangian density.

# 4 Quarkonia

## 4.1 Quarkonia spectroscopy

Since its discovery, charmonia and bottomonia have proven to be powerful tools for strong interaction probing. Due to the high mass of the charm quark ($\approx 1.5$ GeV) and bottom quark ($\approx 4.2$ GeV), it can be described within the language of *non-relativistic potential model* which can be easily tested. Especially interesting are the dynamical properties of its bound states. In this model the asymptotic properties of the strong interaction are embodied in

$$V(r) = -\frac{4}{3}\frac{\alpha_s}{r} + \kappa r, \tag{29}$$

where $\alpha_s$ is the *strong interaction coupling constant*. The first part of equation 29 is dominant at short distances and it is the part motivated by the *perturbative* QCD, whereas the second describes quark confinement in a phenomenological manner. This model is sometimes called *Cornell potential* and all of its free parameters have to be gained from fits of experimental data. In QCD, the coupling constant from equation 26 is denoted by $g$ and by convention is connected to $\alpha_s = g/4\pi$. For illustration of potential from equation 29 for a given values of $\alpha_s$ see figure 22.

The *strong coupling constant* $\alpha_s$ gets larger as the energy scale $\mu$ of the interaction decreases which is caused by the anti-screening effect of the gluon self-interaction

$$\alpha_s(\mu) = \frac{2\pi}{(11 - \frac{2}{3}n_f)\ln\left(\frac{\mu^2}{\Lambda^2}\right)} \tag{30}$$

where $n_f$ is the number of active quark flavours below $\mu$, and $\Lambda$ is the intrinsic QCD scale with a value of around $200 - 400$ MeV. The strong coupling constant diverges when $\mu$ approaches $\Lambda$ and the perturbative QCD calculations cannot be done.

Measurements of the charmonium spectrum below threshold began immediately after their discovery. The first two papers, [Spectrum] and [Spectrum2], submitted by independent groups were received within one week in December 1974. Their results can be seen in the figure 20. The existence of such spectra forever banished the purely mathematical notion of quarks.

Charmonium and bottomium spectroscopy was originally inspired by already well known states of *positronium*. The ground state of positronium has two possible configurations depending on the relative orientations of the electron and positron spins which causes also its different lifetimes. Quarkonia can be characterised by the same numbers as positronium which are total spin of the bound state $S$, the total orbital angular momentum $L$ and

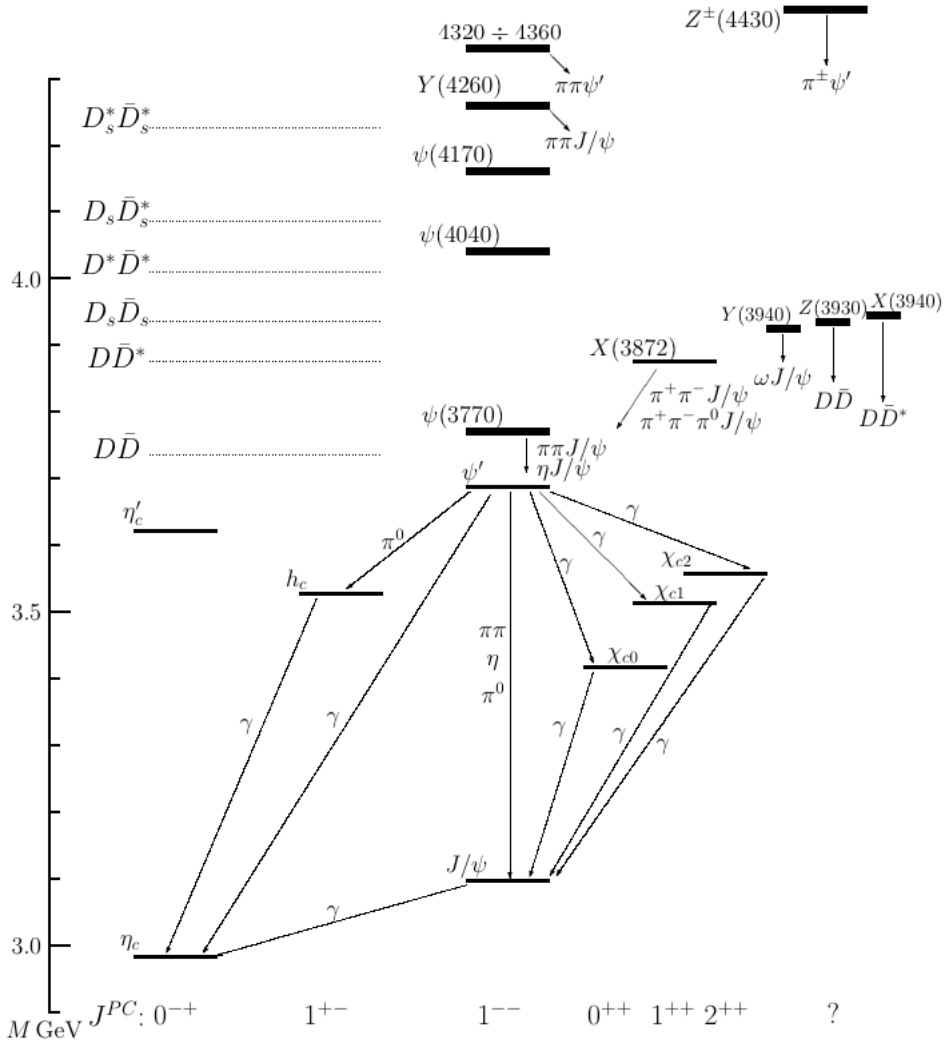


Figure 19: Complete charmonium spectrum.

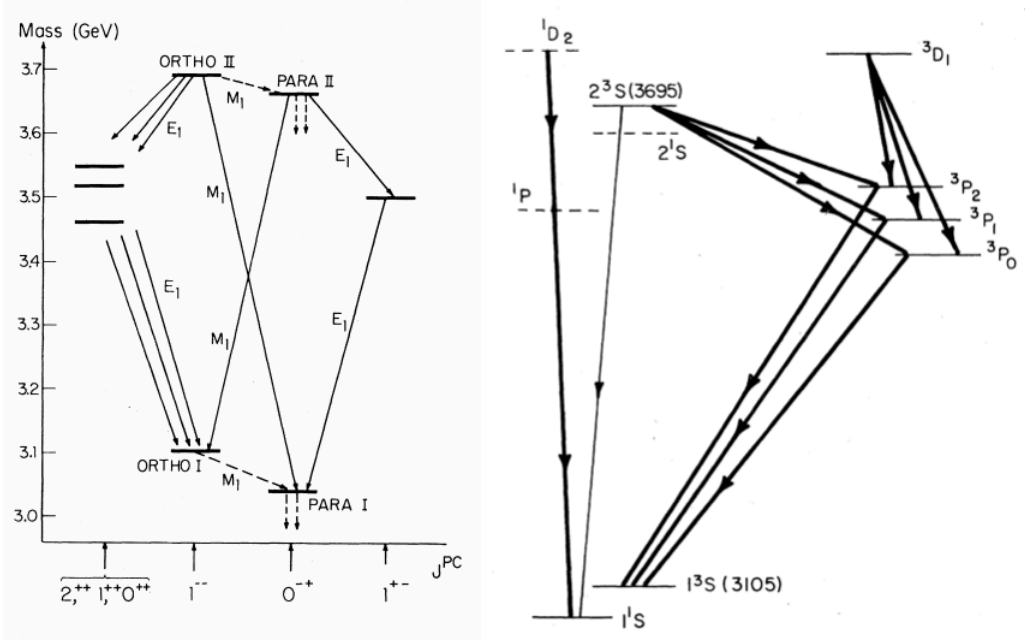


Figure 20: Masses and radiative transitions of charmonium, taken from [Spectrum] (right) and [Spectrum2] (left).

the total angular momentum $J = L + S$. The conserved properties are charge conjugation $C = (-1)^{L+S}$ and parity $P = (-1)^{L+1}$. For overview of basic charmonia states see table 3.

*Para-positronium* is a state with anti-parallel spins denoted as ${}^1S_0$. This singlet state can decay into any even number of gammas but two gamma decay has the largest branching ratio. *Otho-positronium* is a triplet state with electron-positron having the parallel spins. Total angular momentum of ortho-positronium $J$ = 1 and charge conjugation $C$ = -1. In this mode only even number of gammas in final state is possible starting from the most probable number three.

If I assume, as in case of hydrogen atom, that positronium energy levels can be derived from non-relativistic Schrödinger equation

$$E_n = -\frac{\alpha^2 mc^2}{4n^2}, \tag{31}$$

where $n$ is a principal quantum number and $m$ electron mass. Relativistically the levels are split by *spin-orbit interaction* into S,P,... states with different orbital angular momentum $l$, $l < n$ (so called *fine splitting*) and by *spin-spin interaction* into triplet and singlet states (so called *hyperfine splitting*). Positronium (as well as charmonium) constituents have the

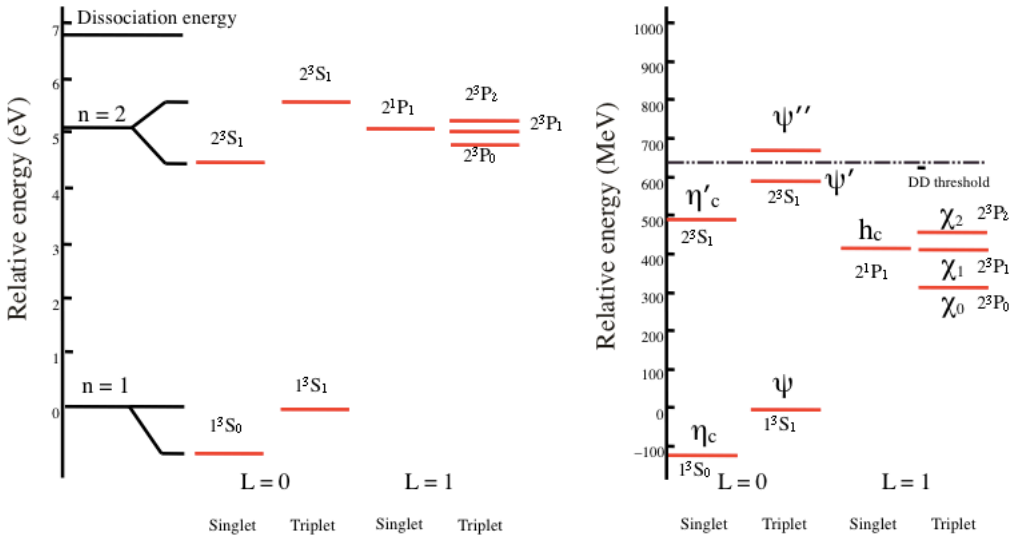


Figure 21: Comparison of positronium (left) and charmonium spectrum (right). Figure was taken from [Comparison].

same mass and therefore magnetic moment of Bohr magneton. This causes that the order of hyperfine and fine splitting is the same

$$\Delta E \sim \frac{\alpha^2 mc^2}{n^3}. \tag{32}$$

In analogy with positronium gross states of heavy quarkonia (bottomonia and charmonia) can be calculated within a non-relativistic QCD framework because quark masses $M$ are large compared to kinetic energy (1.5-4.5 GeV) with $\beta = 0.1 - 0.2$ and also $\Lambda_{QCD} >> M$ which allows us to use non-relativistic treatment but non-relativistic *correction terms* are needed.

Measurements of the properties of heavy quarkonia also provide us with a great opportunity to test very precisely predictions of non-preturbative QCD ($\alpha_s \approx 0.16 - 0.25$), large order perturbation theory, QCD, exotica, confinement, deconfinement and similar effects. Moreover it provides a unique insight into the nature of QCD close to the strong decay threshold.

The similarity between quarkonium and positronium implies that to the strong interac-

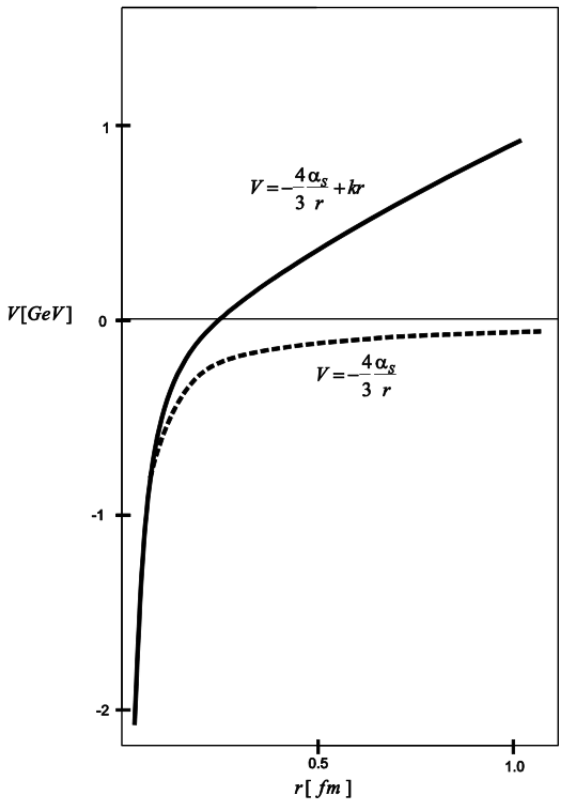


Figure 22: Plot of the QCD potential for $\alpha_s$=0.20 and k = 1 GeV.fm$^{-1}$. Picture was taken from [Perkins].

| Meson | $n^{2S+1}L_j$ | $I^G(J^{PC})$ | Mass [MeV] | Full width |
|---|---|---|---|---|
| $\eta_c$ | $1^1S_0$ | $0^+(0^{-+})$ | $2980.4 \pm 1.2$ | $25.5 \pm 3.4$ MeV |
| $J/\psi$ | $1^3S_1$ | $0^-(1^{--})$ | $3096.916 \pm 0.011$ | $93.4 \pm 2.1$ keV |
| $\chi_{c0}(1P)$ | $1^3P_0$ | $0^+(0^{++})$ | $3414.76 \pm 0.35$ | $10.4 \pm 0.7$ MeV |
| $\chi_{c1}(1P)$ | $1^3P_1$ | $0^+(1^{++})$ | $3510.66 \pm 0.07$ | $0.89 \pm 0.05$ MeV |
| $\chi_{c2}(1P)$ | $1^3P_2$ | $0^+(2^{++})$ | $3556.20 \pm 0.09$ | $2.06 \pm 0.12$ MeV |
| $\psi(2S)$ | $2^3S_1$ | $0^-(1^{--})$ | $3686.093 \pm 0.034$ | $337 \pm 13$ keV |

Table 3: Properties of significant charmonia [PDG].

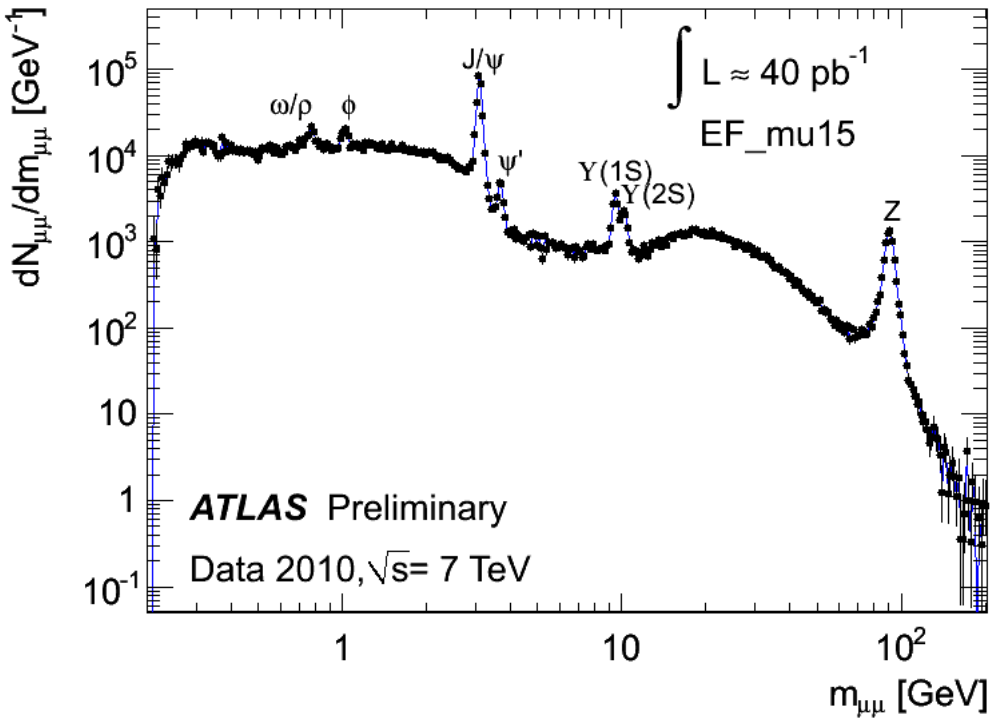


Figure 23: Di-muon invariant mass spectrum for data, from fully combined opposite sign muons in EF_MU15 triggered events with $p_T$ threshold at ~15 GeV, which for consistency is reconfirmed offline for one of the two inner detector-muon spectrometer combined tracks (the other one is required to pass a $p_T$ threshold of 2.5 GeV). The plot is taken from [Dimuon] and corresponds to an integrated luminosity of about 40 pb$^{-1}$.

tion potential (equation 29) should be added more terms reflecting the spin dependence

$$V_{spin}(r) = V_{LS}(r)\left(\vec{L}\cdot\vec{S}\right) + V_T(r)\left[S(S+1) - \frac{(\vec{S}\cdot\vec{r})(\vec{S}\cdot\vec{r})}{r^2}\right] + V_{SS}\left[S(S+1) - \frac{3}{2}\right] \quad (33)$$

where spin-orbit $V_{LS}$ and tensor $V_T$ terms are responsible for the fine structure of the states. The spin-spin term $V_{SS}$, which is for two quarks proportional to $S(S+1)-3/2$, describes the spin splitting on singlet and triplet. This scheme is very, there are plenty of other models and their calculations. But a remarkably successful quarkonium mass predictions can be achieved if properly tuned constants are used.

The leading order of the quarkonium bound state is assumed to be formed of a quark-

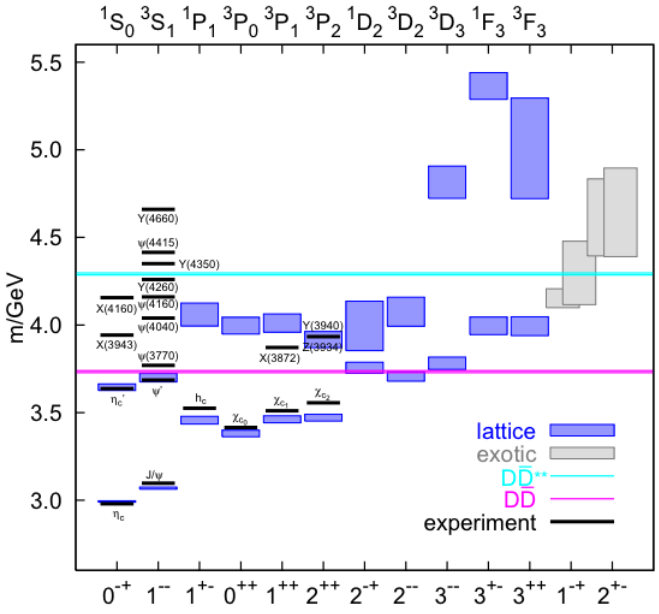


Figure 24: The charmonium spectrum predicted by specific model (for more details please see [CharmModel]) combined with the experimental values.

antiquark pair which must be in an angular momentum state consistent with the quantum numbers of the meson, which leads to an additional spectroscopic notation $n^{2S+1}L_J$ ($n$ here is the principal quantum number).

There are many very specific models that can be compared to today's knowledge of the spectrum, one example is illustrated in the picture 24.

Several peculiar charmonium states were observed in region of 3.9 GeV (see figure 24) at Belle [XYZ]. They were called *XYZ* states and have very different properties and different production precesses. In 2003 at Belle was discovered another XYZ state called X(3872) with mass of $3872.0 \pm 0.6$ MeV, which is very close to the $D^0 D^{0*}$ threshold, and with smaller width than 2.3 MeV. The state was soon confirmed in other experiments. So far there is nothing especially interesting on this lightest "X state" but very unusual is the ratio

$$R_X = \frac{X(3872) \to \pi^+\pi^-\pi^0 J/\psi}{X(3872) \to \pi^+\pi^- J/\psi} = 0.8 \pm 0.3 \tag{34}$$

which cannot be explained by any simple $c\bar{c}$ structure model. The $\pi^+\pi^-$ structure comes from $\rho$ resonance decay and the $\pi^+\pi^-\pi^0$ from $\omega$ decay. The result of ratio 34 is in discrep-

| State | Mass [MeV] | $\Gamma$ [MeV] | $J^{PC}$ | Decay mode |
|---|---|---|---|---|
| X(3872) | $3871.4 \pm 0.6$ | $< 2.3$ | $1^{++}$ | DD* |
| X(3915) | $3914 \pm 3 \pm 2$ | $23 \pm 9$ | ? | D*D* |
| Z(3930) | $3929 \pm 5$ | $29 \pm 10$ | $2^{++}$ | DD |
| X(3940) | $3942 \pm 9$ | $37 \pm 17$ | $1^{++}$ | DD* |
| Y(3940) | $3943 \pm 17$ | $87 \pm 34$ | C = + (?) | $J/\psi\omega$ |

Table 4: Summary of XYZ mesons that can be found in the figure [XYZ].

ancy with expected suppression of $\omega J/\psi$ against the $\rho J/\psi$. This ratio points in direction of isospin mixing and probably both channels, the neutral as well as the charged $DD^*$, are contributing. Very puzzling is recent ratio measurement at Belle that with 90% C.L. gives $R_{X\Gamma} \leq 2.1$ MeV where $R_{X\Gamma}$ stands for

$$R_{X\Gamma} = \frac{\Gamma(X(3872) \to \gamma\psi(2S))}{\Gamma(X(3872) \to \gamma J/\psi)}. \tag{35}$$

The exact nature of the X(3872) is still subject of debates which could be solved with help of the LHC.

In 2005 another resonance named Y(3940) was discovered at Belle and its existence was also later confirmed by other experiments. It was detected near threshold enhancement in the $\omega J/\psi$ invariant mass distribution while measuring the $B \to K\omega J/\psi$. Y(3940) mass was established at $3943 \pm 11 \pm 13$ MeV and a width $\Gamma = 87 \pm 22 \pm 26$ MeV. Its existence was also confirmed by other experiments but in contrary to X(3872) it has not yet been observed in the DD channel. Till today there were identified more similar states and comparison with Colour Evaporation and Colour Singlet models (see chapter 4.2.1) were calculated but theoretical branching ratios are only in a fair agreement with experiment (see [XYZ]).

It illustrates that the DD threshold region is still under investigation and new discoveries of more unusual states are expected. Also more precise measurements to confirm accommodation of new particles in the diagram 24 are needed.

## 4.2 Quarkonia production mechanisms

The structure of this chapter was inspired mostly by [Puzzles], [Price] and [Polarization]. In the last one I also found probably the best motivation for quarkonia studies:

> "Quarkonia represent the most elementary manifestation of the strong binding force and allow us to study crucial open questions: how are quarks confined inside hadrons? How do strong forces generate the properties of particles made of quarks? Can quarks become unbound under extreme conditions (high temperature and density: the quark-gluon plasma), as they existed in the first moments of the universe?"

The Schrödinger equation with one of many existing potential models can be used to obtain the binding energy solutions from which can be derived the mass spectra. The quarkonium wave function $\psi(r) = \psi_{nL}(r) \cdot Y_{Lm}(\theta, \phi)$, where $\psi_{nL}(r)$ and $Y_{Lm}(\theta, \phi)$ are the radial and orbital parts of the this function, have different form for different potentials. These wave functions play an important role in predictions of cross-sections in some models of quarkonium production. Historically, the potential models were an important starting point and they provided us with good understanding of quarkonium spectroscopy. But other theories were needed to explain the production mechanisms and properties of quarkonia.

### 4.2.1 Colour Singlet and Colour Evaporation Models

First on the scene came *Colour singlet model* (CSM). The CSM assumed that if the quarkonium state has some quantum numbers (specially spin and colour) the original quarks were in the same state. The basic CSM assumption is that both quarks resulting in charmonium were produced in a color singlet state. The production rate for each quarkonium state is related to the absolute value of the colour-singlet wave function and its derivatives that are evaluated at zero separations. These quantities are gained by comparing the theoretical expressions for quarkonium decay rates in the CSM to the experimental values. Once this extraction has been carried out, the CSM has no free parameters. The CSM succeeded only in predicting quarkonium production rates at relatively low energies. Moreover, in the case of P-wave state production and higher-orbital-angular-momentum quarkonium states, the CSM leads to uncancelled infrared divergences.

In 1977, the failures of CSM motivated different approach called *Colour evaporation model* (CEM) formulated in [CEM]. CEM is based on the assumption that every produced pair of quark-anti-quark leads to quarkonium if it has an invariant mass smaller than the threshold for production of a pair of open-flavour heavy mesons. The role of colour in selection

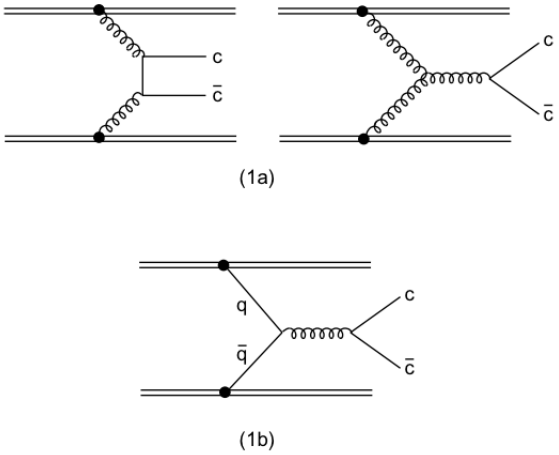


Figure 25: CEM lowest order $c\bar{c}$ production in hadronic collisions through gluon fusion (1a) which is dominant at high energies and quark-antiquark annihilation (1b). Subsequently, the $c\bar{c}$ pair neutralizes its colour by interaction with the collision-induced colour field ("colour evaporation"). During this process, the $c$ and the $\bar{c}$ either combine with light quarks to produce charmed mesons, or they bind with each other to form a charmonium state [QQProduction].

of quarkonia states is ignored. It means that the quark pair is not restricted to being produced in a colour singlet state, but may be produced in an octet state. The numerous soft interactions with colour fields assures that the colour and spin are then modified.

As it was already mentioned in CEM the cross-section $\sigma_{charm}$ for the production of charmonium is proportional to the rate of production of heavy quarks (except for the colour factor $1/9$) in the invariant mass range between twice the heavy quark mass and the threshold, denoted as $2m_D$:

$$\sigma_{charm} = \frac{1}{9}\int_{2m_q}^{2m_D} dm \frac{\mathrm{d}\sigma_{q\bar{q}}}{\mathrm{d}m}. \tag{36}$$

In case of bottomium, the two D mesons have to be switched with B mesons. Dominant Feynman diagrams of charmonium production can be found in the figure 25.

For any particular charmonium state the cross-section $\sigma$ can be projected out from charmonium by multiplication by a density coefficient $\rho$

$$\sigma = \rho\sigma_{charm}. \tag{37}$$

The $\rho$ parameter have to be determined from fits on real data. In fact in CEM the $\rho$ should have no dependence on $\mathrm{p}_T$ or $x$ in the ratios of production cross-sections of various quarko-

nia. In that sense they are universal constants. The soft interactions should cause a randomization of all polarisation effects. Hence the independence on $p_T$ causes the fixed ratio of some charmonium states. According to CEM $\chi(0)$, $\chi(1)$ and $\chi(2)$ production rates through gluon-gluon fusion (see figure 25) should be with respect to their spin (the two-gluon production of charmonia is proportional to $\Gamma_{gg}(2J+1)$) produced with ratio 1:3:5. In Brookhaven [TeV], physicists measured the ratio of direct production of $\chi_c \to J\psi + \gamma$ and obtained the result

$$\frac{\sigma_{\chi c2}}{\sigma_{\chi c1}} = \frac{\chi_{c2} \to J/\psi + \gamma}{\chi_{c1} \to J/\psi + \gamma} = 0.75 \tag{38}$$

which differed significantly from expected number $5/3$. This result proved that CEM is unsuitable for predictions of charmonia production rates at high-energies. Hence, CEM is a phenomenological model so there is no way of calculating the higher order QCD corrections that are important at the high $p_T$ regimes.

### 4.2.2 Soft colour interaction

The *Soft colour interaction* (SCI) model belongs also to the family of phenomenological models such as CEM. It was introduced to explain so called *rapidity gap events* in deep inelastic scattering experiments at HERA (see [DIS]). Later it was scrutinized at hadronic colliders (see [QQTeV]). In SCI the soft interactions are limited by a scale up to which they are taken into account and the soft processes are affecting only colour due to the lack of possibilities to deal with them in rigorous way. The events are simulated in one of the Monte Carlo generators with only one parameter $R$ which has to be extrapolated from data.

In SCI a $q\bar{q}$ colour octet state may transform into a colour singlet state (or vice-versa). The SCI charmonium cross section can be derived similarly to the one of CEM model but it has to be modified because of the soft processes. The cross-section for charmonia state $\sigma_{charm}$ can be put in very elegant way

$$\sigma_{charm} = \frac{\Gamma_{charm}}{\sum_i \Gamma_i} \sigma_{q\bar{q}}, \tag{39}$$

where $\Gamma_i = (2J_{charm}+1)/n_i$ is a partial width. This model is in a better agreement with available data but again it has problems in high-$p_T$ regions.

### 4.2.3 Colour octet mechanism and NRQCD

The *Colour Octet Mechanism* (COM) differs from the previous models as it does not cling to the idea that the quantum numbers of original quarks have to agree with the numbers of

final meson. On the contrary, the quark pairs that are produced in the hard process do not have to have the quantum numbers of final quarkonium. They can evolve into a quarkonium state through soft gluon radiations in the late phase of the production process.

This idea does not sound very different from SCI or CEM but it a differs significantly in used "language". The COM was the first theory for quarkonia production mechanisms that was rigorously formulated within a field theory called Non-relativistic Quantum Chromodynamics. The effective field theory allows us to separate the non-perturbative and perturbative parts within NRQCD which makes the calculations much more feasible.

Quarkonia are again assumed to be non-relativistic, which can be expressed in three scales: the *typical kinetic energy* $m_q v^2$ where $v$ is a relative velocity that quark has in a bound state, *typical momentum transfer* $m_q v$ and the quark mass $m_q$. The energy scale is responsible for the splitting among various quarkonium states and it can be indentified with $\Lambda_{QCD}$. The perturbative QCD usability is defined by quark mass. The evolution of $q\bar{q}$ pair into quarkonium is determined by the momentum scale. The work in a non-relativistic region these conditions have to be met:

$$\left(m_q v^2\right)^2 \ll \left(m_q v\right)^2 \ll m_q^2 \tag{40}$$

The relation $\Lambda_{QCD}$ is proportional to $m_q v^2$ from which approximate values of $v^2$ can be separated for charmonia ($\sim$ 0.25) and bottomonia ($\sim$ 0.09). Very general NRQCD lagrangian can be derived from QCD lagrangian 26

$$\mathcal{L}_{QCD} = \mathcal{L}_{light} + \mathcal{L}_{heavy} + \delta\mathcal{L}. \tag{41}$$

The $\mathcal{L}_{light}$ denotes

$$\mathcal{L}_{light} = -\frac{1}{2}\mathrm{TR}\left[G_{\mu\nu}G^{\mu\nu}\right] + \bar{q}i\gamma^{\mu}D_{\mu}q, \tag{42}$$

where the field strength tensor $G^{\nu\mu}$ describes the free gluon field and the free light quark fields. The $\mathcal{L}_{heavy}$ stands for

$$\mathcal{L}_{heavy} = \psi^{\dagger}\left(iD_t + \frac{\vec{D}^2}{2m_q}\right)\psi + \chi^{\dagger}\left(iD_t - \frac{\vec{D}^2}{2m_q}\right)\chi, \tag{43}$$

where $\psi$ denotes anihilation and $\chi$ denotes creation operator of heavy quark or antiquark. The significant difference from QCD lagrangian is that these operators are only *two* component spinors. The $D_t$ and $\vec{D}$ terms denote the time and space components of $D_{\mu} = \partial^{\mu} + ig_s A^{\mu}$ respectively. The $A^{\mu} = (\phi, \vec{A})$ is a gauge field. The $\delta\mathcal{L}$ term incorporates all possible operators that are consistent with symmetries of QCD. The leading relativistic corrections

are bilinear in the heavy quark fields

$$\begin{aligned}\delta\mathcal{L}_{corrections} = &\frac{C_1}{8m_q^3}\left(\psi^\dagger(\vec{D}^2)^2\psi - \chi^\dagger(\vec{D}^2)^2\chi\right)\\ &+\frac{C_2}{8m_q^2}\left[\psi^\dagger\left(\vec{D}\cdot g\vec{E} - g\vec{E}\cdot\vec{D}\right)\psi + \chi^\dagger\left(\vec{D}\cdot g\vec{E} - g\vec{E}\cdot\vec{D}\right)\chi\right]\\ &+\frac{C_3}{8m_q^2}\left[\psi^\dagger\left(i\vec{D}\times g\vec{E} - g\vec{E}\times i\vec{D}\right)\cdot\vec{\sigma}\psi + \chi^\dagger\left(i\vec{D}\times g\vec{E} - g\vec{E}\times i\vec{D}\right)\cdot\vec{\sigma}\chi\right]\\ &+\frac{C_4}{2m_q}\left[\psi^\dagger\left(g\vec{B}\cdot\vec{\sigma}\right)\psi - \chi^\dagger\left(g\vec{B}\cdot\vec{\sigma}\right)\chi\right]\end{aligned} \tag{44}$$

where $\vec{E}$ is electric colour field, $\vec{B}$ magnetic colour field and $\vec{\sigma}$ spin operator. In fact these operators are given by relations $E^i = G^{0i}$ and $B^i = \frac{1}{2}E^{ijk}G^{jk}$. With the help of additional terms, the NRQCD results can be in principle reproduced to any desired accuracy.

The total cross section for inclusive production of a quarkonia state $A$ can be expressed as

$$\mathrm{d}\sigma(kl \to A + X) = \sum_{n_i} \mathrm{d}\sigma_{q\bar{q}}\,(kl \to q\bar{q}(n_i) + X)\,\langle\mathcal{O}^A(n_i)\rangle, \tag{45}$$

where the matrix element is defined as

$$\langle\mathcal{O}^A(n_i) = \sum_{\lambda,X}\langle 0|\chi^\dagger\kappa_{n_i}\phi|A(\lambda)X\rangle\langle A(\lambda)X|\chi^\dagger\kappa'_{n_i}\phi|0\rangle \tag{46}$$

which is summed over all polarisations $\lambda$ and light hadrons $X$. The factors $\kappa_{n_i}$ and $\kappa'_{n_i}$ specifies the quark-anti-quark pair, its angular momentum, spin and colour.

In the equation 45, the total cross sections is obtained as a sum over all possible quantum numbers of states $n_i$ that contains a quark-anti-quark pair. According to the NRQCD factorisation hypothesis, the cross section is a sum of short distance coefficients that describe creation of particular $q\bar{q}$ pair which is multiplied with matrix element for a given process. Now it is obvious that the separation of non-perturbative processses from the perturbative hard ones is possible.

### 4.2.4 Power counting

The colour octet matrix elements cannot be predicted within NRQCD and thus they are free parameters of the model. This makes the NRQCD very universal. Many processes can be calculated, including the photoproduction and DIS. But there are rules how to determine

the relative importace of such terms. This procedure is called power counting or velocity scaling and it supposes that a general matrix element can be scaled approximately like

$$\langle \mathcal{O}[^{2S+1}L_j^{(1,8)}]\rangle \sim v^{3+2L+2E_1+4M_1} \tag{47}$$

where $E_1$ and $M_1$ are minimum numbers of chromoelectric ($\Delta L = \pm 1$ and $\Delta S = 0$) and chromomagnetic ($\Delta L = \pm 0$ and $\Delta S = \pm 1$) transitions that are needed to reach the dominant quarkonium Fock state from the $^{2S+1}L_J^{(1,8)}$ state (the (1,8) factor denotes whether the quarkonium is in colour singlet or colour octet state). The octet terms should be suppressed relatively to the singlet states because of the $E_1$ and $M_1$ transition that are always needed to get this final state.

In NRQCD any charmonium state is defined in a Fock space and such state can be obtained with the infinite sum of contributions of states in this space. If double expansion of $\alpha_s$ and $v$ is applied then it can be decided which terms from this series can be neglected and which will contribute the most. For example a charmonium state $J/\psi$ can be represented as follows

$$\begin{aligned} J/\psi =& O(1)|q\bar{q}[^3S_1^1]\rangle + O(v)|q\bar{q}[^3P_j^8]g\rangle + O(v^2)|q\bar{q}[^3S_1^{(1,8)}]gg\rangle \\ &+ O(v^2)|q\bar{q}[^3S_1^{(8)}]g\rangle + \dots \end{aligned} \tag{48}$$

The Colour single model demonstrated in calculations of P-wave decays in next to leading order a divergent behaviour. The octet state provided additional Fock states and in NRQCCD the contribution of these states solved the problem of infrared divergences. In P-wave the leading terms of Fock state decomposition are

$$|\chi_J\rangle = O(1)|q\bar{q}[^3P_J^1]\rangle + O(v)|q\bar{q}[^3S_1^8]g\rangle. \tag{49}$$

The contribution from COM to CSM singlet state is represented by a pair of $c\bar{c}$ in colour octet state and in configuration $^3S_1$ to which one gluon is added. The gluon plays here an important role as it changes the quantum numbers of the quark pair when it is emitted. This enables an evolution into a singlet P-wave state. Note that even if the production through colour octet is suppressed by powers of $v$, these octet contributions could play important role in quarkonium production. The difference in conceptions of how to get to the singlet state is illustrated in the figure 26. Both diagrams are infrared divergent but in the final sum they are cancelled with other divergent diagrams. Thus the NRQCD matrix elements are incorporated in Monte Carlo generators used at ATLAS.

The NRQCD can be very well tested with high $p_T$ quarkonia that are produced at LHC. The

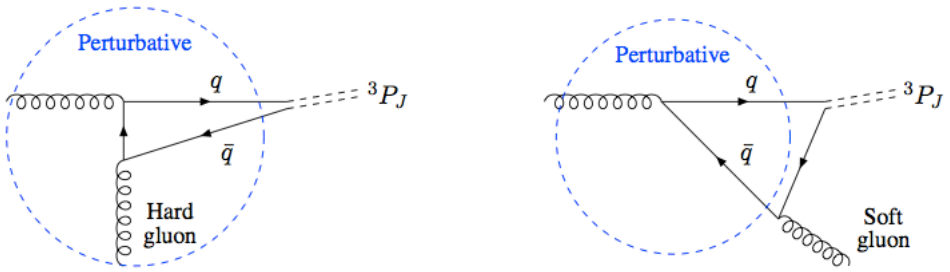


Figure 26: The production of $^3P_J(1)$ state in CSM (left). The same process that is possible only in NRQCD: $^3S_1(8)$ to $^3P_J(1)$ (right). The figure was taken from [Price].

gluon fragmentation is the dominant production channel if quarkonium $p_T$ is significantly larger than its mass. Such gluon is close to its mass shell, which means it is transversally polarised. According to theory such gluon should lead to a polarised quark-antiquark pair and this charmonium polarisation can be measured. The polarisation analyses performed at colliders are usually transformed into measurements of the angular distribution as a function of the polar angle with respect to the chosen spin-quantization axis. Normally it has the form

$$1 + \alpha \cos^2 \theta. \tag{50}$$

The parameter $\alpha = 1$ corresponds to 100% transverse polarization and $\alpha = -1$ corresponds to 100% longitudinal polarization of measured quarkonia.

In theory some parameters like the polar asymmetry $\alpha$ can be expressed in terms of ratios of polarized quarkonium cross sections. These ratios can be sometimes less sensitive than the production cross sections to the theoretical uncertainties from quantities such as the factorization scale, the renormalization scale, the heavy-quark mass, and the NRQCD long-distance matrix elements. The polar asymmetry parameter does not give complete information about the polarization state of produced quarkonium. Its significance very much depends on the the orientation of the spin-quantization axis. To determine the relevant production mechanisms, the high-statistics measurements of $J/\psi$ and $\chi_{cJ}$ polarizations are needed.

Moreover the COM can be used to describe quarkonium production in other processes, such as deep inelastic scattering or electron-positron annihilation. There exist calculations that support the NRQCD approach by showing that NRQCD factorisation holds in NLO processes. There are many other theories like $k_T$ *factorisation* approach which at high energies describes the gluon distribution function in QCD. In the phenomenology of strong interactions at high energies, it is necessary to describe the QCD evolution of the gluon distri-

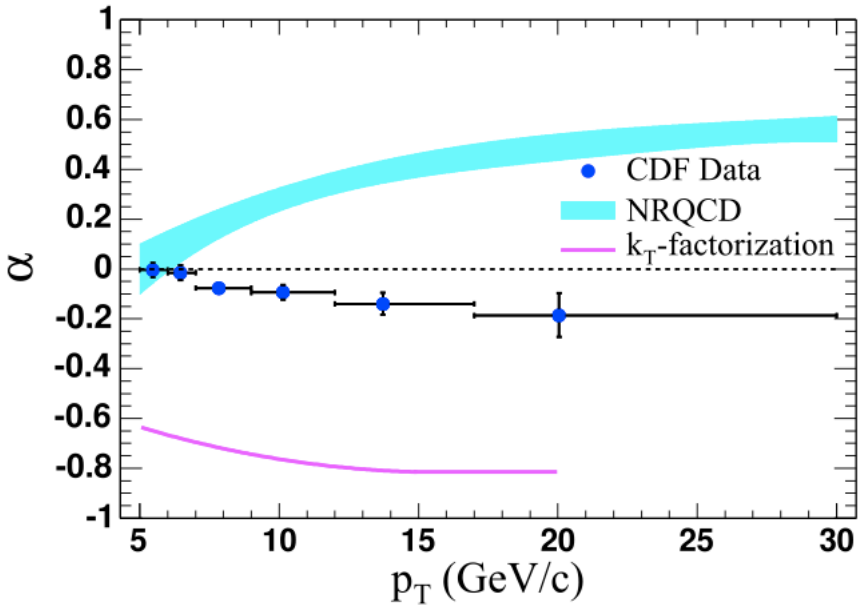


Figure 27: The dependence of polarization parameter $\alpha$ for prompt $J/\psi$ production at $p_T$ in $p\bar{p}$ collisions at $\sqrt{s} = 1.96$ TeV. The points are recorded data from the Collider Detector at Fermilab (CDF), the band is the prediction taken from LO NRQCD factorization, and the line is the prediction from $k_T$ factorization. The figure was taken from [Alpha].

bution functions of the colliding particles starting from some scale $\mu_0$, which controls the non-perturbative regime, to the typical scale $\mu$ of the hard-scattering processes, which is typically of the order of the transverse mass $m_T = \sqrt{m^2 + |\vec{p}_T^2|}$ of the produced particle (or hadron jet) with (invariant) mass $M$ and transverse two-momentum $p_T$. In the region of very high energies, the typical ratio $x = \mu/\sqrt{S}$ becomes very small, $x \ll 1$. This leads to large logarithmic contributions of the type $[\alpha_s \ln(1/x)]^n$, which need to be resummed. This is conveniently done by adopting the high-energy factorization scheme, which also known as the $k_T$-factorization approach, in which the incoming t-channel gluons have a finite transverse two-momentum $k_T$ and are off mass shell [kT].

# 5 Analysis of J/Psi + photon continuum

In this section I would like to presents the results of the $J/\psi + \gamma$ continuum analysis being performed on the ATLAS 2011 data. This analysis is carried out for B-Physics working group at CERN and will be later published as ATLAS Note. I present one of the first steps taken in studies of the charmonia states (see table 5) at the ATLAS experiment. The continuum with the $\chi_{c1}(1P)$ and $\chi_{c2}(1P)$ with some hints on $\chi_{c0}(1P)$ charmonium states can be observed. This work is a continuing effort to measure the cross sections of the $\chi_c$ triplet and to further study the continuum.

## 5.1 ROOT

For my analysis I chose to use ROOT which is a framework for data processing developed at CERN. It is commonly used in high-energy physics to analyse data and perform visualizations. I have reprocessed my data (see table 6) into a ROOT file which is a file in compressed binary form. The original datasets contained collections of J/$\psi$ event candidates reconstructed using the JPsiFinder algorithm. Electromagnetic calorimeter clusters and conversion candidates were also present in the data.

For this analysis I used about 983 $pb^{-1}$ of 2011 ATLAS data. The data were from taking periods D, E, F2, F3 and G. For all details see table 6.

I preferred the ROOT ntuple tree data structure as ROOT can work much better with huge amounts of data that are commonly used in such analyses. These data are then usually analysed using the C++ macros.

The ROOT framework provides a number of classes, grouped into several class categories, that can be found on the related web-page [ROOT].

I especially appreciated the RooFit library which provided me a very good toolkit for data modeling. This package was originally released in 1999 for the BaBar collaboration and the vast majority of BaBar results was fitted using this framework. Since 2005 RooFit is a standard part of ROOT releases. It provided me with a flexible environment for fitting, it offers more tan 20 most frequently used basic probability density functions like Breit-Wigner, Crystal Ball, Gaussian and many others. It also assures that the probability density functions does not differ in structure but only in parameters.

## 5.2 J/Psi reconstruction

To $J/\psi$ identification was used $J/\psi \to \mu^+\mu^-$ channel which has branching fraction $\Gamma_{J/\psi}/\Gamma$ = 5.93 $\pm$ 0.06 %. In general, momenta of muons can be measured by the Inner Detector

and the Muon Spectrometer. In my analysis I used information from both. The resolution of muons with $p_T < 6$ GeV is very good due to a precise Inner Detector measurements of low $p_T$ muons and the Muon Spectrometer is used for confirmation of identification of such muons.

To combine the muon tracks that are reconstructed in the Inner Detector and the Muon Spectrometer, the Muon Identification STACO software package is in place. This package helped me to associate segments and tracks found in the Muon Spectrometer with the corresponding Inner Detector tracks. Hence it uses information from EM calorimeter in order to identify muons at their production vertex with optimum parameter resolution.

An experimental measurement of $\chi_c$ production in hadronic collisions can offer a step towards unique insight into the nature of charmonium hadro-production and the strong interaction in general as I have described in previous chapters.

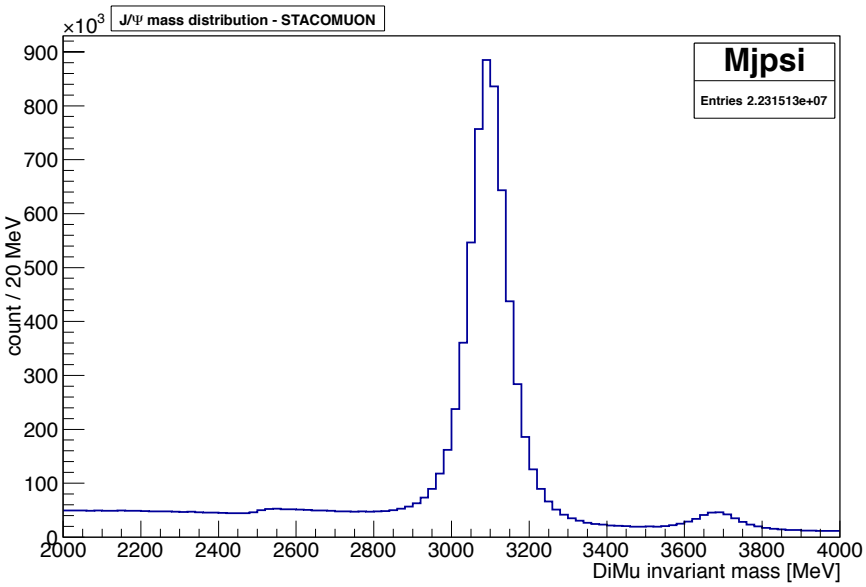


Figure 28: The Di-muon invariant mass. $J/\psi$ peak dominates the mass spectrum at 3096 MeV and radial excitation $\psi(2s)$ at 3686 MeV. For this analysis, mass windows of M(J/$\psi$) PDG $\pm$ 100 MeV was used.

Study of $\chi_{cJ}$ production is also important to determine the contribution of the $\chi_{cJ}$, that decays through this channel (or so-called radiative decays), to the inclusive $J/\psi$ cross sec-

tion. These decays are expected to account for around 30% to 40% of the $J/\psi$ production in pp collisions at the LHC. The more detailed study of $\chi_{cJ}$ production can offer a step toward the extraction of the cross section for direct $J/\psi$ production from the total prompt cross section.

I applied these cuts on $J\psi$:

- $|y| < 2.5$
- muon $p_t > 4$ GeV
- muon $\eta < 2.5$
- $J/\psi$ $\chi^2 < 100$
- $|M(\mu^+\mu^-) - M(J/\psi(PDG))| \pm 100$ MeV

Approximately $J/\psi$ 5.46 x $10^6$ candidates passed these criteria.

## 5.3 Photon reconstruction

There are two types of reconstructed photon data available for ATLAS: conversions and clusters in the electromagnetic calorimeter. The electron and photon identification in ATLAS relies on rectangular cuts using variables which deliver good separation between isolated electrons and photons and fake signatures from QCD jets. These variables include information from the calorimeter and tracker. Photons are reconstructed from the sliding window clusters if there is no reconstructed (electron) track matched to the cluster. They are called unconverted photon candidates, if there is a reconstructed conversion vertex matched to the cluster they are designated as the converted photon candidates [Photon].

Concerning photons reconstructed in the calorimeter, three photon authors (algorithms) are available:

| | | |
|---|---|---|
| Author | 0x04 (4 dec.) | Photon reconstructed by standard cluster-based algorithm. |
| Author | 0x10 (16 dec.) | Photon that is duplicated with electron. |
| Author | 0x80 (128 dec.) | Photon reconstructed by SW CaloTopo35 seeded clusters. |

In the figure 29 the invariant mass spectrum of $\chi_c$ candidates is shown for various authors.

The list of applied cuts on $\gamma$:

- photon $p_T > 1$ GeV
- photon $\eta < 2.5$ GeV

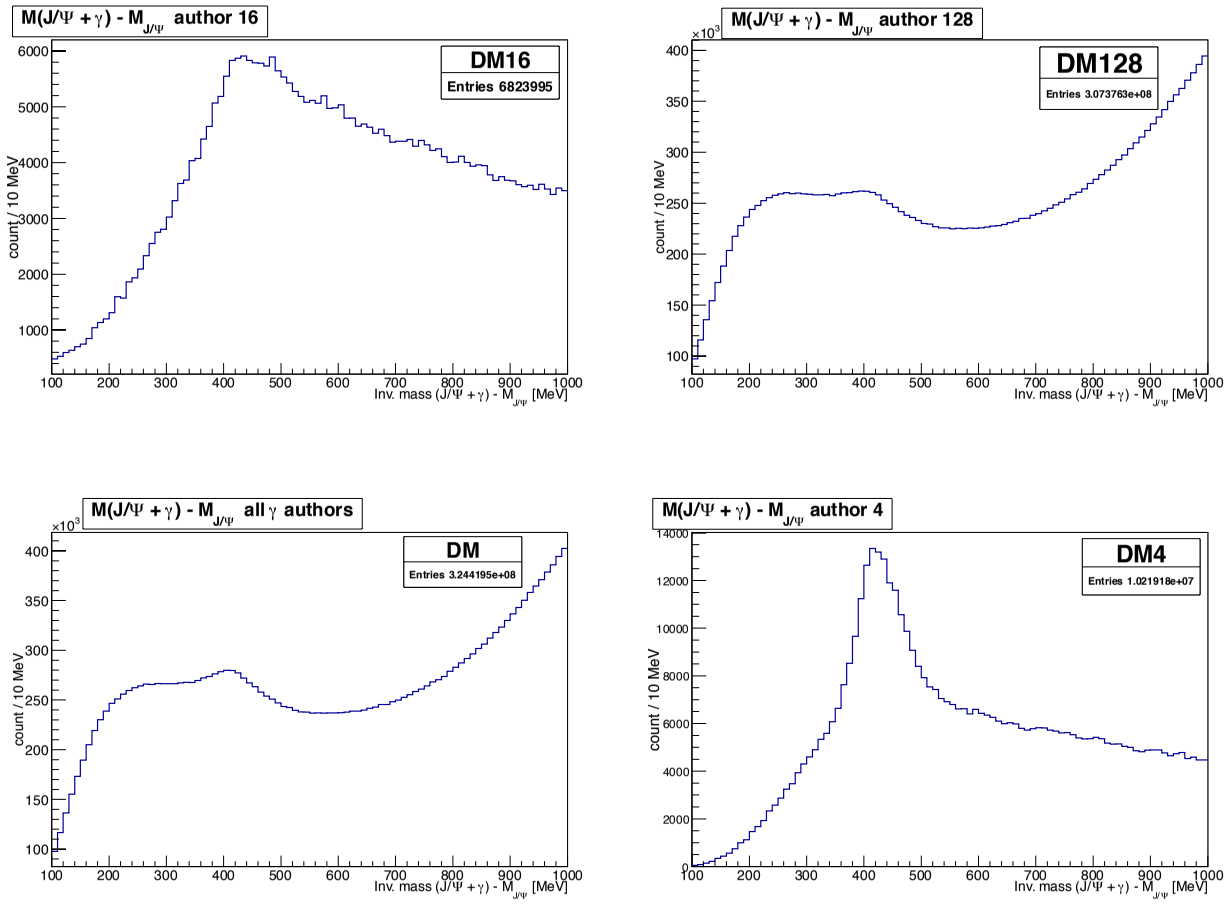


Figure 29: The invariant mass spectrum of $\chi_c$ candidates. The DM figure contains combined data using all algorithms for photon reconstruction in calorimeter. In the figure DM4 I used photons reconstructed by standard cluster-based algorithm. In the DM16 I used photons that were duplicated with electrons. In the figure DM128 are depicted photons reconstructed by SW CaloTopo35 seeded clusters.

Approximately 296 000 $\gamma$ passed these criteria.
For conversions:

- at least 6 hits in Pixel and SCT
- conversions $\eta < 2.3$
- conversions $p_T > 1$ GeV

The best results according to figure 29 can be achieved only with the photon candidates number 4 that are reconstructed using the standard-base cluster algorithm. The transverse momenta distributions of all photons and photon candidates number 4 are depicted in the figures 30 and 31.

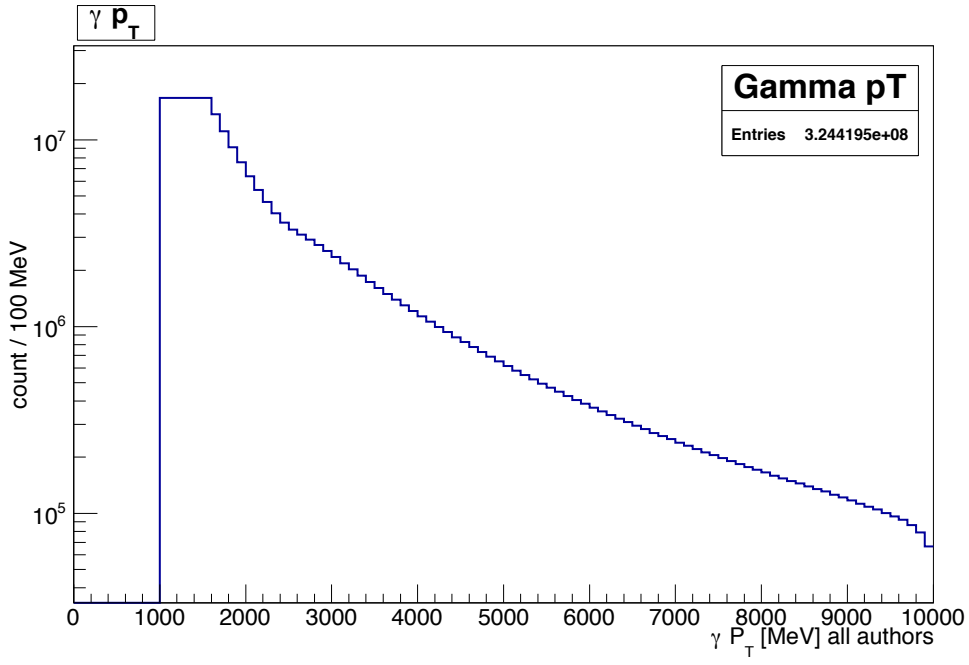


Figure 30: The $p_T$ distribution of all photon candidates.

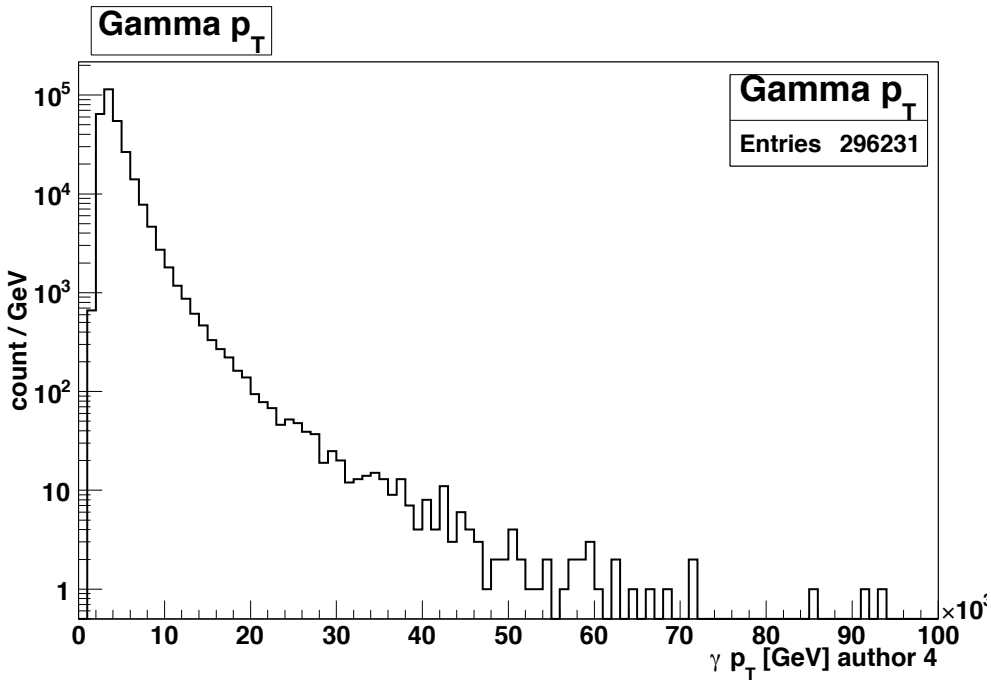


Figure 31: The $p_T$ distribution of photons candidates reconstructed by standard-base cluster algorithm that I used in my analysis.

## 5.4 Charmonia reconstruction

Only charmonium that can be easily reconstructed in the di-muon channel is the J/$\psi$ and it's radial excitation $\psi$(2S) due to their large decay branching fraction into a muon pair. JpsiFinder is an Athena (ATLAS data analysis framework) package which performs a vertex fit on a pair of muon and antimuon, it's output are ntuples easily processed by ROOT. Polarization of the charmonia and it's effect on the reconstruction efficiency is neglected.

## 5.5 Triggers

Di-Muon Trigger where LVL1 muons are confirmed by the HLT. This provides a primary trigger for B-physics analyses such as B->mumu and B->mumuX. In this analysis it is used to trigger channels with a charmonium in the final state.

To determine $J/\psi$ I used a di-muon topological trigger EF_2mu4_Jpsimumu. This algo-

| State | Mass [MeV] | Width [MeV] | $I^G(J^{PC})$ | $\Gamma_{J/\psi+\gamma}/\Gamma$ [%] |
|---|---|---|---|---|
| $\chi_{c0}(1P)$ | $3414.75 \pm 0.31$ | $10.5 \pm 0.8$ | $0^+(0^{++})$ | $1.17 \pm 0.08$ |
| $\chi_{c1}(1P)$ | $3510.66 \pm 0.07$ | $0.88 \pm 0.05$ | $0^+(1^{++})$ | $34.4 \pm 1.5$ |
| $\chi_{c2}(1P)$ | $3556.20 \pm 0.09$ | $1.95 \pm 0.13$ | $0^+(2^{++})$ | $19.5 \pm 0.8$ |

Table 5: Summary of resonances observable in $J/\psi + \gamma$ continuum.

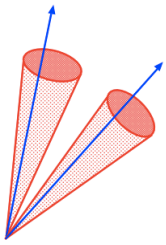

Figure 32: Regions of interest and how they are selected by the EF_2mu4_Jpsimumu trigger.

rithm was developed for the B-physics program at the ATLAS experiment. For ATLAS is important to achieve a high trigger efficiency for low-$p_T$ di-muon events, keeping an acceptable trigger rate. ATLAS developed two separate approaches for triggering on di-muon events to determine charmonium resonances such as a $J/\psi$. The first approach is to start from a di-muon trigger selected by the LVL1 trigger which is the one that is used at EF_2mu4_Jpsimumu. The other is based on LVL2 trigger.

EF_2mu4_Jpsimumu is seeded by two RoI from LVL1 muon trigger as it is illustrated in the figure 32.

If the muon coming from the Interaction Point (IP) hast transverse momentum above a given threshold a LVL1 selects these tracks. LVL1 trigger provides a first estimation of the parameters $\eta$, $\phi$ and $p_T$ that are corresponding to a Region of Interest (RoI). This algorithm is hardware based and hence it takes into account energy losses in the calorimeter.

A precise understanding of the trigger efficiency is essential for a wide range of analyses, especially cross section measurements. The method of estimating the di-muon trigger efficiency data-driven and was based on Bayes Theorem:

$$P(Trigger\_2\mu) = \frac{P(Trigger\_1\mu) \times P(Trigger\_2\mu|Trigger\_1\mu)}{P(Trigger\_1\mu|Trigger\_2\mu)} \tag{51}$$

where $P(Trigger\_2\mu|Trigger\_1\mu)$ is ratio between all the events that fired the $Trigger\_1\mu$ and all event that fired the $Trigger\_1\mu$ and the $Trigger\_2\mu$. The $P(Trigger\_1\mu|Trigger\_2\mu)$

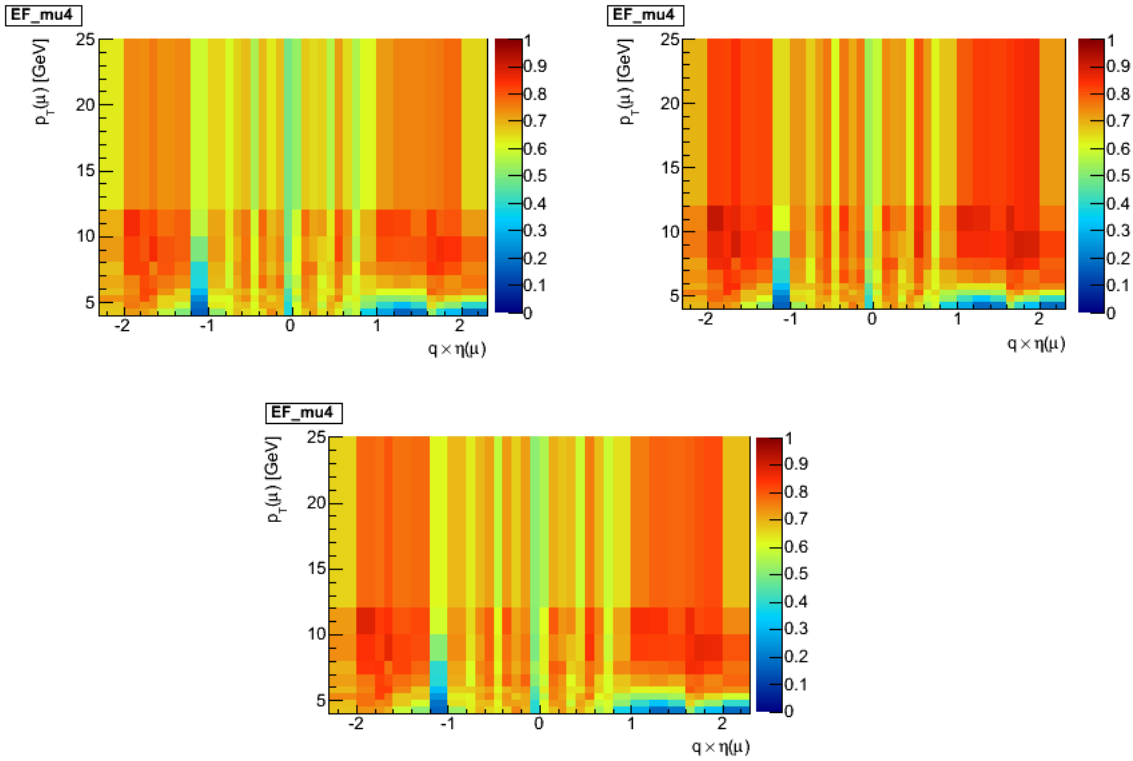


Figure 33: The muon trigger efficiencies for $p_T$ and $\eta$ range used in the analysis. The picture show different efficiencies for the $p_T$ and $\eta \times q$ regions. This single muon trigger is used for di-muon trigger efficiency calculation.

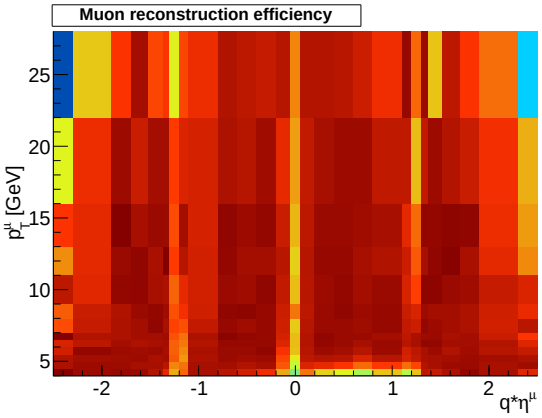


Figure 34: The single muon reconstruction efficiency.

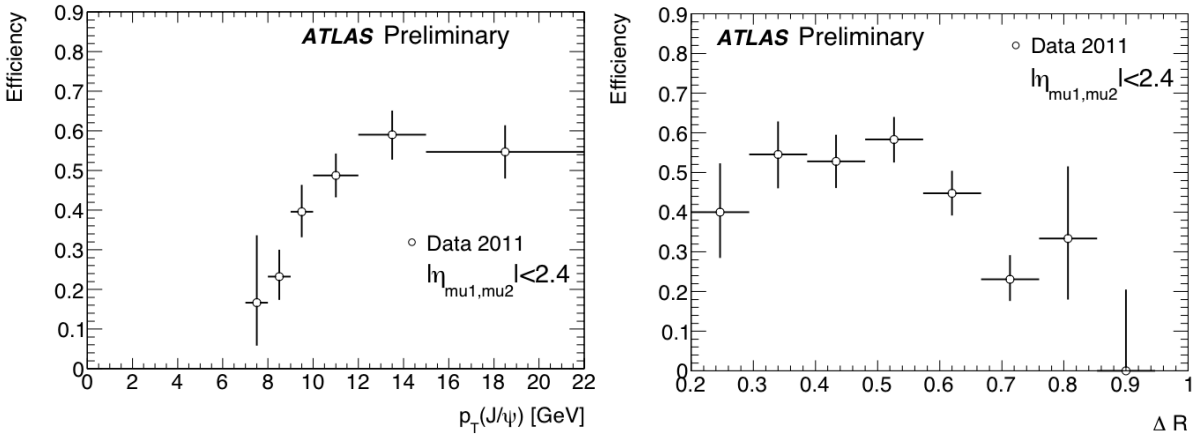


Figure 35: Dependence of the EF_2mu4_Jpsimumu efficiency on the $J/\psi$ candidate $p_T$ (left). Dependence of the EF_2mu4_Jpsimumu efficiency on the $\mu_1$ reconstructed $p_T$ (right). The figures were taken from [Eff].

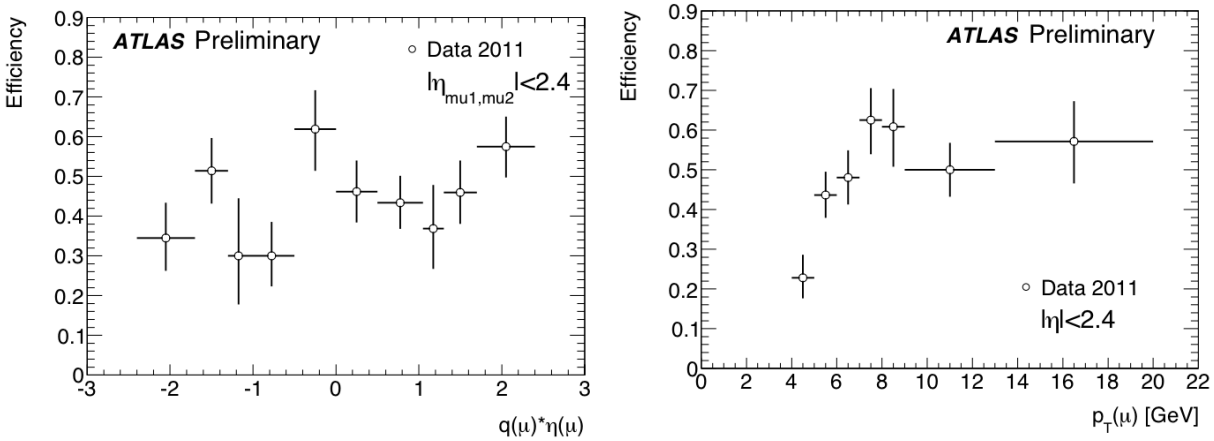


Figure 36: Dependence of the EF_2mu4_Jpsimumu efficiency on the $\mu_1$ reconstructed $q.\eta$ (left). Dependence of the EF_2mu4_Jpsimumu efficiency on the angular separation $\Delta$R (right). The figures were taken from [Eff].

is the ratio between all events that fired the $Trigger\_1\mu$ and the $Trigger\_2\mu$ and all events that fired the $Trigger\_1\mu$.

The single muon trigger efficiency was obtained by a standard tag and probe method.

The efficiency of the di-muon trigger is computed as the efficiency of two single muon triggers with corrections, provided by the ATLAS B-Physics group which can be found in the figure 33.

The efficiency of photon reconstruction provided by the B-Physics group turned out to be unsuitable and I will evaluate it again in the near future.

## 5.6 Signal modelling

The measured width of the J/$\psi$ resonance is much larger than the physical width due to the limited detector momentum resolution. J/$\psi$ signal can be modelled as a Dirac function convoluted with a Gaussian, where Gaussian represents smearing due to the detector resolution. In the case of $\chi_c$, this smearing is combined with the uncertainty of the reconstructed photon or conversion energy. The individual peaks of each $\chi_{c1}, \chi_{c2}$ resonances are not resolved due to the fact that distance between means of $\chi_{c1}$ and $\chi_{c2}$ is comparable to the detector resolution. The most significant of the fit is provided by following formula

$$S = c_1.G_1(\chi_{c1}) + (1 - c_1).G_2(\chi_{c2}), \tag{52}$$

where $G_1(\chi_{c1})$ and $G_2(\chi_{c2})$ denotes the $\chi_{c1}$ Gaussian and $\chi_{c2}$ Gaussian. The two For some of the results also third Gaussian for $\chi_{c0}$ was used.

## 5.7 Background modelling

For the background modelling seemed to be the most optimal choice the Novosibirsk function which is commonly used in B-physics analysis

$$N = \exp\left\{\frac{\xi\sqrt{\xi^2+1}(x-x_1)\sqrt{2\ln 2}}{\sigma_p\left(\sqrt{\xi^2+1}-\xi\right)^2\ln\left(\sqrt{\xi^2+1}+\xi\right)} + \rho\left(\frac{x-x_i}{x_p-x_i}\right)^2 - \ln 2\right\}, \tag{53}$$

where $N$ is a function of $x, x_p, \sigma_p, \xi, \rho_1, \rho_2$ and for $x < x_1$ it $\rho = \rho_1$ and $x_i = x_1$. For $x \geq x_2$ is $\rho = \rho_2$ and $x_i = x_2$ with

$$x_{1,2} = x_p + \sigma_p\sqrt{2\ln 2}\left(\frac{\xi}{\sqrt{\xi+1}} \mp 1\right). \tag{54}$$

The parameters represents: $x_p$ denotes the peak position in the distribution, $\sigma_p$ is the parameter of the width $\sigma_p = \mathrm{FWHM}/2\sqrt{2\ln 2}$, $\xi$ is the peak asymmetry parameter and $\rho_{1,2}$ describe the extent of the left and the right tails.

It is in fact a modified Gaussian with an extra tail parameter that skews the Gaussian into an asymmetric shape with a long tail on one side and a short tail on the other.

## 5.8 Fit results

I've performed a binned maximal likelihood fit on the data in the J/Psi $p_T$-bins 8-12 GeV, 12-15 GeV, 15-20 GeV and 20+ GeV. Results can be seen on figures 38 and 39 in the middle row.

The variable bkg_peak, bkg_tail and bkg_width, fraction, nbkg, nsigma can be associated with variables from the equation 53. First $p_T$ bin was done using gaussians for $\chi_{c1}$ and $\chi_{c2}$ due to the lower statistics. For the rest of the results the third $\chi_{c0}$ gaussian had to be added. Systematics of the muon reconstruction and triggering can be evaluated. It is around 5% for all $p_T$ bins for both muon reconstruction and trigger.

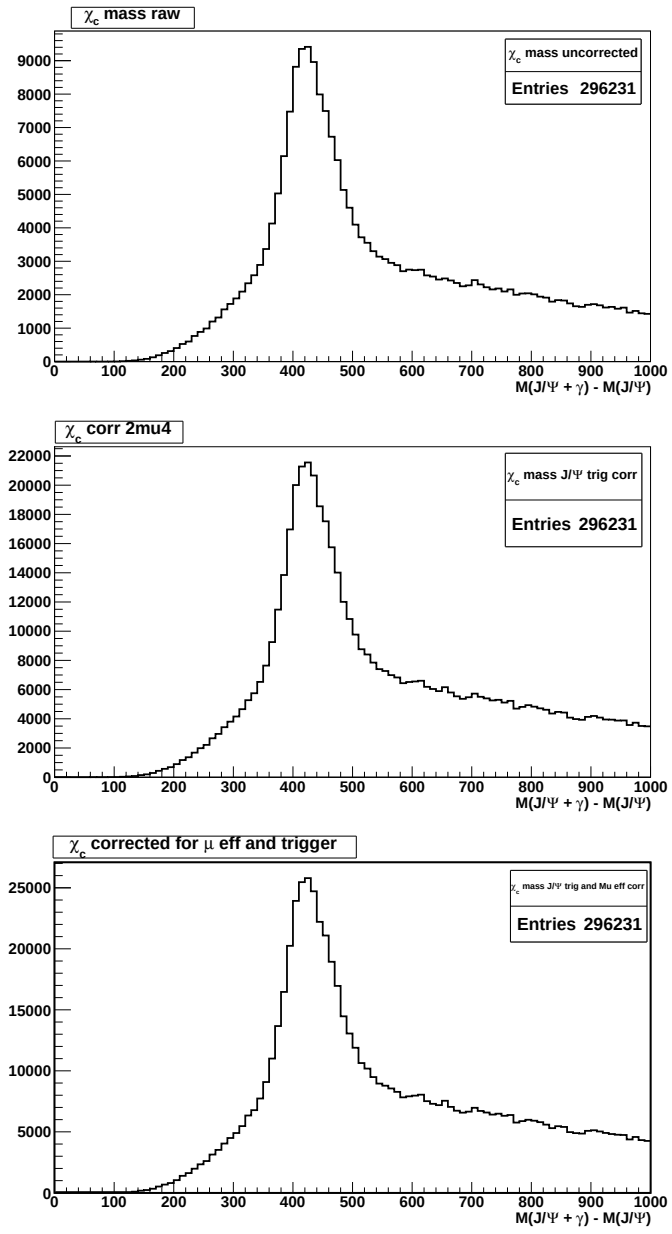


Figure 37: $\chi_c$ Mass spectra for uncorrected muons and J/$\psi$, correction on J/$\psi$ trigger and for corrected J/$\psi$ in combination with correction on muon reconstruction efficiency.

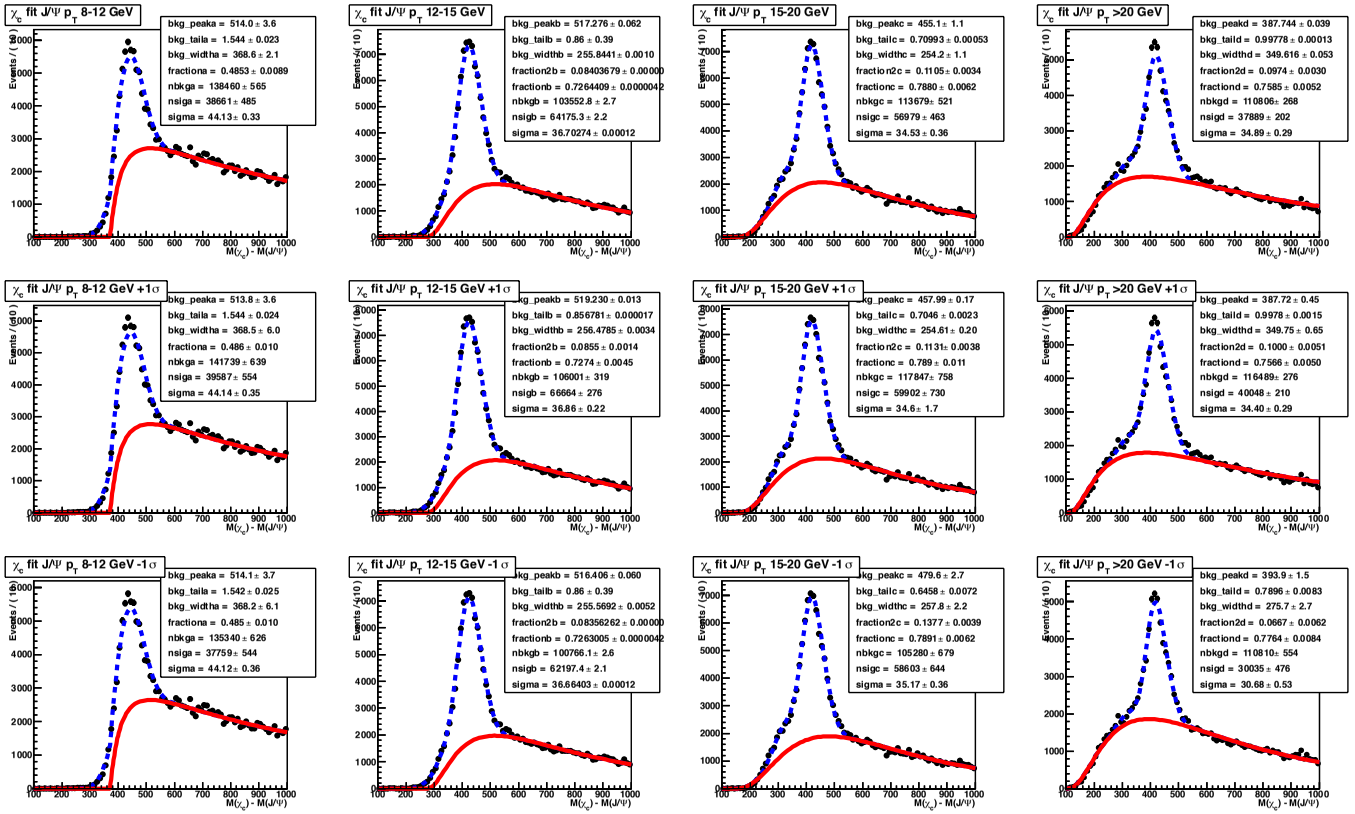


Figure 38: $\chi_c$ fit divided in different J/$\psi$ $p_T$ bins with applied trigger reconstruction efficiencies. In the second row are depicted results with corrections which were produced by variation of the correction factor by + $1\sigma$. In the third row the variation of the correction factor is + $1\sigma$.

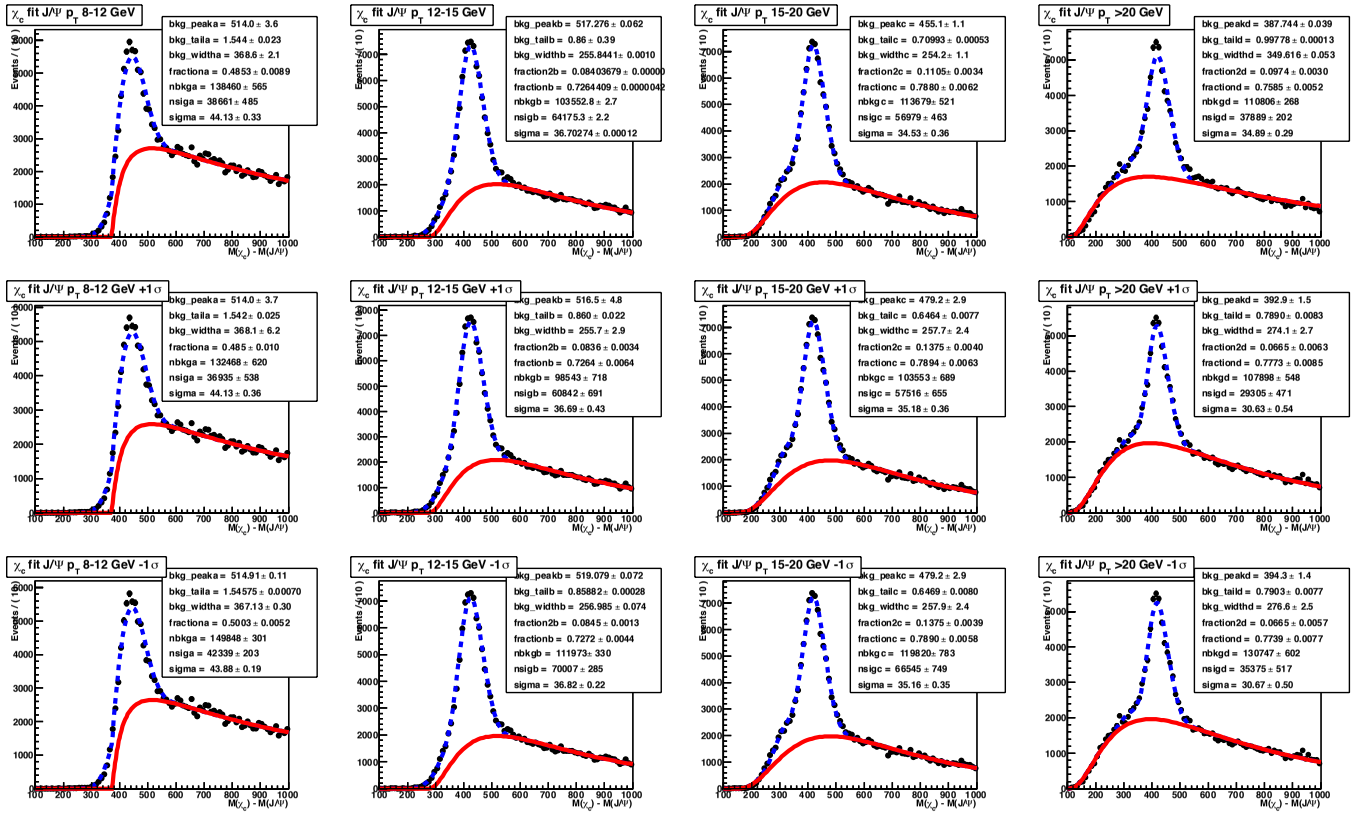


Figure 39: $\chi_c$ fit divided in different J/$\psi$ $p_T$ bins with applied muon reconstruction efficiencies. In the second row are depicted results with corrections which were produced by variation of the correction factor by + 1$\sigma$. In the third row the variation of the correction factor is + 1$\sigma$.

Selected runs

| Run number | Int. $\mathcal{L}$ [pb$^{-1}$] | Run number | Int. $\mathcal{L}$ [pb$^{-1}$] | Run number | Int. $\mathcal{L}$ [pb$^{-1}$] |
|---|---|---|---|---|---|
| Period D | | Period E | | Period G | |
| 180481 | 26.17 | 180614 | 4.34 | 182726 | 6.50 |
| 180448 | 1.54 | 180636 | 29.73 | 182747 | 30.38 |
| 180400 | 20.64 | 180664 | 4.22 | 182766 | 5.47 |
| 180309 | 12.10 | 180710 | 16.50 | 182787 | 37.65 |
| 180242 | 7.69 | **sum** | **54.79** | 182796 | 32.22 |
| 180241 | 5.91 | | | 182879 | 6.29 |
| 180225 | 20.10 | Period F2, F3 | | 182886 | 4.89 |
| 180164 | 23.96 | 182161 | 3.37 | 182997 | 4.36 |
| 180153 | 10.83 | 182284 | 18.55 | 183003 | 46.61 |
| 180149 | 5.14 | 182346 | 2.41 | 183021 | 27.70 |
| 180144 | 4.43 | 182372 | 18.07 | 183038 | 1.46 |
| 180139 | 9.95 | 182424 | 25.20 | 183045 | 18.76 |
| 180124 | 9.79 | 182449 | 4.45 | 183054 | 9.64 |
| 180122 | 6.77 | 182450 | 2.08 | 183078 | 2.49 |
| 179939 | 5.50 | 182454 | 11.64 | 183079 | 1.62 |
| 179938 | 1.71 | 182455 | 1.90 | 183081 | 45.03 |
| 179804 | 10.11 | 182456 | 22.50 | 183127 | 13.32 |
| 179771 | 1.84 | 182486 | 29.10 | 183127 | 13.32 |
| 179739 | 3.58 | 182516 | 11.40 | 183129 | 7.68 |
| 179725 | 2.72 | 182518 | 3.15 | 183130 | 20.29 |
| 179710 | 6.79 | 182519 | 5.54 | 183216 | 31.04 |
| **sum** | **197.28** | **sum** | **159.37** | 183272 | 13.38 |
| | | | | 183286 | 30.92 |
| | | | | 183347 | 30.76 |
| | | | | 183391 | 23.08 |
| | | | | 183407 | 42.62 |
| | | | | 183412 | 1.31 |
| | | | | 183426 | 29.34 |
| | | | | 183462 | 46.93 |
| | | | | **sum** | **571.73** |

Table 6: Selected runs for cross-section analysis with total integrated luminosity of 983 pb$^{-1}$.

# 6 Conclusions

In the first chapter of my thesis I shortly described the Large Hadron Collide. In the following chapter the ATLAS detector is introduced and the ATLAS subdetectors are discussed with focus on the muon system and the Inner Detector which are important for my analysis.

In the third chapter chapter an overview of the particle physics and the Standard model is presented. The historical development that led to the quark model and the Quantum Chromodynamics is introduced and phenomenons that are related to resonances are discussed.

In the next chapter physics related to quarkonia, their spectroscopy and various theoretical descriptions of their production mechanisms channels are discussed in detail.

The last part of this thesis concerns the data analysis in the muon + photon stream which I did on behalf of the ATLAS B-physics working group. The 2011 ATLAS data were used with accumulated statistics of about 1.2 $\text{fb}^{-1}$. Main part of analysis is preparation for the measurement of $\chi_c$ production cross section in the $\chi_{cJ} \rightarrow J/\psi + \gamma$ decay channels for which the evaluation of the muon trigger part is mostly finished. The cross section will be computed as a fiducial cross section with $p_T > 4$ Gev and $|\eta| < 2.5$.

# Appendix A

**Propagators:**

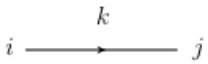


$$i\,\delta_{ij}\frac{(\not{k}+m)}{k^2-m^2+i\epsilon}$$

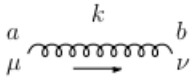


$$\frac{-i\,\delta_{ab}}{k^2+i\epsilon}\left[g_{\mu\nu}-(1-\eta)\frac{k_\mu k_\nu}{k^2}\right]$$

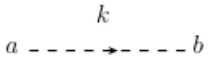


$$\frac{-i\,\delta_{ab}}{k^2+i\epsilon}\,,$$

$$\eta \text{ fixes the gauge: } \eta = \begin{cases} 1, & \text{Feynman gauge} \\ 0, & \text{Landau gauge} \end{cases}$$

**Vertices:**

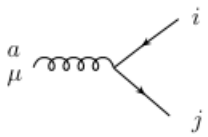


$$ig_s\gamma_\mu T^a_{ji}$$

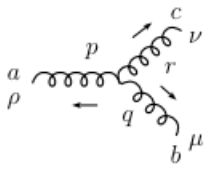


$$-g_s f^{abc}\left[(p-q)_\nu\, g_{\rho\mu}+(q-r)_\rho\, g_{\mu\nu}+(r-p)_\mu\, g_{\nu\rho}\right]$$

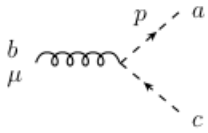


$$g_s\, f^{abc} p_\mu \text{ } (p_\mu \text{ outgoing})$$

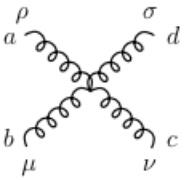


$$\begin{aligned} &-ig_s^2 f^{abe} f^{cde}\left(g_{\rho\nu}g_{\mu\sigma}-g_{\rho\sigma}g_{\mu\nu}\right) \\ &-ig_s^2 f^{ace} f^{bde}\left(g_{\rho\mu}g_{\nu\sigma}-g_{\rho\sigma}g_{\mu\nu}\right) \\ &-ig_s^2 f^{ade} f^{cbe}\left(g_{\rho\nu}g_{\mu\sigma}-g_{\rho\mu}g_{\sigma\nu}\right) \end{aligned}$$

## References


[AccComp] *CERN coll.:* **LHC accelerator complex [online].** http://te-epc-lpc.web.cern.ch/te-epc-lpc/machines/pagesources/Cern-Accelerator-Complex.jpg [cit. 2012-05-15].

[Alpha] *CDF Collaboration:* **Polarizations of $J/\psi$ and $\psi(2S)$ Mesons Produced in ppbar Collisions at 1.96 TeV.** Phys.Rev.Lett.99:132001 (2007). arXiv:0704.0638v2.

[Asymptotic] *Politzer, D. H.:* **Reliable Perturbative Results for Strong Interactions?** Phys. Rev. Lett. 30, 1346-1349 (1973).

[Asymptotic2] *Gross, D. J.; Wilczek, F.:* **Ultraviolet Behavior of Non-Abelian Gauge Theories.** Phys. Rev. Lett. 30, 1343-1346 (1973).

[ATLAS] *Grillo, A.:* **The ATLAS Experiment [online].** http://scipp.ucsc.edu/personnel/atlas.html [cit. 2012-05-15].

[Calorimetry] *ATLAS experiment:* **ATLAS photos [online].** http://www.atlas.ch/photos/calorimeters-combined-barrel.html [cit. 2012-05-15].

[CharmModel] *Bali, G. S.:* **Charmonium spectroscopy and mixing with light quark and open charm states from $n_F = 2$ lattice QCD.** arXiv:1110.2381.

[CEM] *Fritzsch, H.:* **Producing heavy quark flavors in hadronic collisions – A test of quantum chromodynamics.** Phys. Lett. B 67, 217-221 (1977).

[Colour] *Bardeen, W. A.; Fritzsch, H.; Gell-Mann, M.:* **Light-Cone Current Algebra, $\pi^0$ Decay, and $e^+e^-$ annihilation.** arXiv:hep-ph/0211388v1 (1973).

[Comparison] *Voloshin, M. B.:* **Charmonium.** arXiv:0711.4556v3 (2008).

[Delta] *Ashkin, J.; Blaser, J. P.; Feiner, F.; Gorman, J. and Stern, M. O.:* **Total Cross Sections of 135-Mev to 250-Mev Negative Pions in Hydrogen.** Phys. Rev. 93 (1954), 1129.

[Dimuon] *ATLAS coll.:* **Combined Muon Performance Public Results [online].** https://twiki.cern.ch/twiki/bin/view/AtlasPublic/MuonPerformancePublicPlots#AnchorPlots2011 [27.7.2012].

[DIS] *Edin, A; Ingelman, G. and Rathsman, J.:* **Soft Colour Interactions as the Origin of Rapidity Gaps in DIS.** arXiv:hep-ph/9508386.

[Eff] *Picazio, A. on behalf of the ATLAS coll.:* **A measurement of the ATLAS Di-Muon Trigger Efficiency in proton-proton collisions at $\sqrt{s}$ =7 TeV.** arXiv:1201.5752v1 (2012).

[Feyn] *Feynamn, R.P.:* **Very high-energy collisions of hadrons.** Phys. Rev. Lett. 23, 1415–1417 (1969).

[GIM] *Glashow, S.L; Iliopoulos, J. and Maiani, L.* **Weak Interactions with Lepton-Hadron Symmetry.** Phys. Rev. D 2, 1285–1292 (1970).

[Han] *Han, M. Y.; Nambu Y.:* **Three-Triplet Model with Double SU(3) Symmetry.** Phys. Rev. 139, B1006-B1010 (1965).

[Inner] *CERN 2009 - ATLAS experiment:* **Inner Detector [online].** http://atlasexperiment.org/inner_detector.html [cit. 2012-05-13].

[J] *Aubert J.J. and coll.:* **Experimental observation of a heavy particle J.** Phys. Rev. Lett. 33, 1404-1406 (1974).

[Kem] *Kemmer, N.:* **The Particle Aspect of Meson Theory.** Proc. R. Soc. Lond. A 1939 173, 91-116.

[Kstar] *Alston, M. and coll.:* **Resonance in the K-$\pi$ system.** Phys. Rev. Lett. Volume 6 (1961), 300.

[kT] *Hansson, M.; Jung, H. and Jönsson, L.:* **Calculation of Heavy Quark Production in electron-positron and photon-photon collisions using the kt-factorization approach.** Theoretical Physics 4. (2003). Lund University, Sweden.

[LHC] *Evans, L.; Bryant P.:* **LHC Machine.** Journal of Instrumentation, Vol. 3 (2008 JINST 3 S0800), August 2008.

[Lum] *ATLAS coll.:* **Total Integrated Luminosity in 2011 [online].** https://twiki.cern.ch/twiki/bin/view/AtlasPublic/LuminosityPublicResults [cit. 2012-03-27].

[Mesons] *Fermi, E.; Young, C. N.:* **Are mesons elementary particles?** Phys. Rev. 76, 1739–1743 (1949).

[MuTrig] *Aloisio, A. and coll.:* **The trigger chambers of the ATLAS muon spectrometer: production and tests** Proceedings of the 10th International Vienna Conference on Instrumentation. December 2004.

[Nambu] *Nambu, Y.:* **Proc. Second Coral Gables conference on symmetry principles at high energy.** University of Miami, 1965.

[Ne] *Ne'eman Y.:* **Derivation of strong interaction from a gauge invariance.** Nuclear Physics 26, 222–229 (1961).

[Omega] *Barnes, V. E. and coll.:* **Observation of a Hyperon with Strangeness Minus Three.** Phys. Rev. Lett. 12, 204-206 (1964).

[Para] *Greenberg, O. W.:* **Spin and Unitary-Spin Independence in a Paraquark Model of Baryons and Mesons.** Phys. Rev. Lett. 13, 598-602 (1964).

[Photon] *The ATLAS Collaboration:* **Electron and photon reconstruction and identification in ATLAS: expected performance at high energy and results at 900 GeV** ATLAS-CONF-2010-005 (2010).

[PDG] *J. Beringer et al.:* **The Review of Particle Physics.** Particle Data Group, Phys. Rev. D86, (2012).

[Perkins] *Perkins, D. H.:* **Introduction to High Energy Physics.** Cambridge: Cambridge University Press; 4th edition (April 24, 2000). ISBN-13 978-0521621960.

[Phi] *Bertanza, L. and coll.:* **Possible Resonances in the $\Xi\pi$ and $K\bar{K}$ Systems.** Phys. Rev. Lett. Volume 9 (1962).

[PhysOut] *Bosman, M. on behalf of the ATLAS coll.:* **ATLAS Detector Status and physics startup Plans.** IFAE, Barcelona, E-08193, Spain. (Prepared for 34th International Conference on High Energy Physics, Philadelphia, 2008).

[Pi] *Occhialini, G. P. S.; Powell, C. F.:* **Nuclear Disintegrations Produced by Slow Charged Particles of Small Mass.** Nature 159, 186–190 and 160, 453–456 (1947).

[Polarization] *Faccioli, P.:* **Questions And Prospects in Quarkonium Polarization Measurements from proton-proton to nucleus-nucleus collisions.** arXiv:1207.2050v1.

[Prel] *Nambu, Y.:* **Systematics of hadrons.** Published in De-Shalit, A. and coll.: Preludes in theoretical physics in honor of V. F. Weisskopf. Amsterdam: North-Holland publishing company, 1966.

[Price] *Price, D.:* **Studies of quarkonium production and polarisation with early data at ATLAS.** PhD Thesis submitted at Lancaster University. 2008.

[Psi] *Augustin, J.-E. and coll.:* **Discovery of a narrow resonance in $e^+e^-$ annihilation.** Phys. Rev. Lett. 33, 1406-1408 (1974).

[Puzzles] *Brambilla N. and coll.:* **Heavy quarkonium: progress, puzzles, and opportunities.** arXiv:1010.5827v3.

[QCD] *Chýla, J.:* **Quarks, partons and Quantum Chromodynamics.** Scriptum for a course in the phenomenology of the quark-parton model and Quantum Chromodynamics, 2008. Charles University in Prague and AS CR.

[QQProduction] *Gavai, R. and coll:* **Quarkonium Production in Hadronic Collisions.** arXiv:hep-ph/9502270 (1995).

[QQTeV] *Edin, A; Ingelman, G. and Rathsman, J.:* **Quarkonium Production at the Tevatron through Soft Colour Interactions.** arXiv:hep-ph/9705311.

[Quarks] *Gell-Mann, M.:* **A schematic model of baryons and mesons.** Physics Letters 8, 214-215 (1964).

[Rior] *Riordan M.:* **The Discovery of Quarks.** Science Vol. 256, 1287-1293, (1992).

[ROOT] *The ROOT development team [online]:* **ROOT analysis framwork.** http://root.cern.ch/drupal/ [28.7.2012].

[Sakata] *Sakata, S.:* **On a composite model for the new particles.** Prog. Theor. Phys. Vol. 16 No. 6 686-688 (1956).

[Spectrum] *Appelquist, T. and coll.:* **Spectroscopy of the New Mesons.** Phys. Rev. Lett. 34, 365-369 (1975).

[Spectrum2] *Eichten, E. and coll.:* **Spectrum of Charmed Quark-Antiquark Bound States.** Phys. Rev. Lett. 34, 369-372 (1975).

[TeV] *Abulencia, A. et al:* **Measurement of $\sigma_{\chi_{c2}} B(\chi_{c2} \to J/\psi\gamma)/\sigma_{\chi_{c1}} B(\chi_{c1} \to J/\psi\gamma)$ in pp Collisions at $\sqrt{s}$ = 1.96 TeV.** arXiv:hep-ex/0703028v1 (2007).

[TDR] *ATLAS collaboration:* **Technical Design Report Volume 1.** CERN/LHCC 99-14 (1999).

[TDR2] *ATLAS collaboration:* **Technical Design Report Volume 2.** CERN/LHCC 99-15 (1999).

[Top] *Abe, F. and CDF Collaboration:* **Observation of Top Quark Production in $p\bar{p}$ Collisions with the Collider Detector at Fermilab.** Phys. Rev. Lett. 74, 2626-2631 (1995).

[Trig] *Picazio A. on behalf of ATLAS collaboration:* **A Measurement of the ATLAS Di-Muon Trigger Efficiency in Proton-Proton Collision at $\sqrt{s}$ =7 TeV.** arXiv:1201.5752v1.

[Upsilon] *Herb, S. W. and coll.:* **Observation of a Dimuon Resonance at 9.5 GeV in 400-GeV Proton-Nucleus Collisions.** Phys. Rev. Lett. 39, 252-255 (1977).

[Upsilon2] *Innes, W. R. and coll.:* **Observation of Structure in the $\Upsilon$ Region.** Phys. Rev. Lett. 39, 1240-1242 (1977).

[Width] *Aaltonen, T. and the CDF coll.:* **Search for new physics in $t\bar{t} + E_T \rightarrow b\bar{b}q\bar{q}q\bar{q} + E_T$ final state in $p\bar{p}$ collisions at $sqrts$ =1.96 TeV.** arXiv:1107.3574v2 (2011).

[XYZ] *Choi, S.-K. and Belle Coll.:* **Observation of a Narrow Charmoniumlike State in Exclusive $BB^{\pm} \rightarrow K^{\pm}\pi^{+}\pi^{-}J/\psi$ decays.** Phys. Rev. Lett. 91, 262001 (2003) [6 pages].

[Y-M] *Mills, R.; Yang C. N.:* **Conservation of Isotopic Spin and Isotopic Gauge Invariance.** Phys. Rev. 96, 191–195 (1954).

[Zweig] *Zweig, G.:* **An SU(3) model for strong interaction symmetry and its breaking.** CERN-TH-412.

[8-way] *Gell-Mann M.:* **Symmetries of Baryons and Mesons.** Phys. Rev. 125, 1067–1084 (1962).